

CONSORTIUM MATERIALS TECHNOLOGY for demonstration and development of thermal energy processes

Critical corrosion phenomena in power generation from biomass

Identification of chlorine resistant high temperature coatings/materials

Participants

HTC, Chalmers: Torbjörn Jonsson, Jesper Liske and Andreas Slomian DONG Energy and DTU: Kristian Vinter Dahl, Anette Nørgaard Hansson, Saeed Kiamehr and Trine Nybo Lomholt

KME-511

Critical corrosion phenomena in power generation from biomass

Identification of chlorine resistant high temperature coatings/materials

Participants

HTC, Chalmers: Torbjörn Jonsson, Jesper Liske and Andreas Slomian DONG Energy and DTU: Kristian Vinter Dahl, Anette Nørgaard Hansson, Saeed Kiamehr and Trine Nybo Lomholt

Preface

The project has been performed within the framework the fifth stage of the material technology research programme KME.

KME, Consortium Materials technology for demonstration and development of thermal Energy processes, was established 1997 on the initiative of the Swedish Energy Agency. In the consortium, the Swedish Energy Agency, seven industrial companies and 18 energy companies participate. The programme stage has been financed with 60.2 % by participating industrial companies and with 39.8 % by Swedish Energy Agency. The consortium is managed by Elforsk.

The programme shall contribute to increasing knowledge to forward the development of thermal energy processes for various energy applications through improved expertise, refined methods and new tools. The programme shall through material technology and process technology developments contribute to making electricity production using thermal processes with renewable fuel more effective. This is achieved by

- Forward the industrial development of thermal processes through strengthened collaboration between industry, academy and institutes.
- Build new knowledge and strengthen existing knowledge base at academy and institutes
- Coordinate ongoing activities within academy, institutes and industry

KME's activities are characterised by long term industry relevant research and constitutes an important part of the effort to promote the development of new energy technology with the aim to create an economic, environmentally friendly and sustainable energy system.

Abstract

Combustion of biomass results in a much more corrosive fireside environment compared to the combustion of fossil fuels such as coal. The corrosive properties of the fuel have mainly been attributed the high alkali chlorine content. By studying field exposed samples and performing thermodynamic calculations the Ni-Al material system was identified as a possible alkali chloride resistant coating/material. The Ni-Al system was in addition tested through laboratory exposures where the Ni₂Al₃ coating formed a protective aluminium rich scale in the presence of KCl.

Sammanfattning

Alkalikloridinducerad korrosion är ett betydande hinder för att nå KMEs mål att erhålla en ångtemperatur på 600°C i biomasseldade pannor. Detta eftersom alkalikloridinducerad korrosion har identifierats som en begränsande faktor i denna typ av pannor. Ett sätt att övervinna detta problem är att använda korrosionsbeständiga beläggningar/material. I det aktuella projektet har överhettarprover från biomasseldade pannor undersökts. Resultaten har kompletterats med termodynamiska beräkningar och screeningförsök i syfte att identifiera möjliga korrosionsbeständiga beläggningar. Det mest lovande systemet (Al - Ni) har dessutom undersökts genom laboratorieexponeringar.

Karakterisering av TP347HFG-överhettarprover (rostfritt stål) visade att materialet inte kunde bilda en skyddande kromoxid i en verklig överhettarmiljö efter långa exponeringstider. Istället för skyddande kromrik oxid återfanns en tjock järnrik oxid ovanför en FeCrNi-oxid på alla prover. På vissa delar återfanns även en omfattande korngränsattack långt ner i materialet. Resultaten från den ingående undersökningen av fältprover kombinerades med termodynamiska beräkningar för att välja det mest lovande beläggningsmaterialet. Termodynamiska utvärderingar utförda med hjälp av Thermo-Calc visade tillsammans med screeningexperiment att Ni-Almaterialet har störst potential i alkalikloridrika miljöer och då specifikt Ni₂Al₃-fasen som valdes för testerna. Aluminiserade prover producerades vid DTU via packcementering. Denna aluminisering bildade ett \sim 30 μ m tjockt skikt av Ni₂Al₃.

Al-Ni prover har dessutom undersökts och jämförts med ett vanligt 18-8 rostfritt stål (304L) genom laboratorieexponeringar. AlNi-systemet visar en stor potential för att bilda en skyddande aluminium rik oxid i den alkalikloridmiljö som används under exponeringarna i laboratoriet. Resultaten har genererat intresse hos pannägare och förhoppningen finns att gå vidare med fältstudier. Målet med projektet har därmed uppfyllts.

Nyckelord: Alkaliklor inducerad korrosion, korrosionsbeständiga beläggningar/material, överhettare livstid

Summary

Alkali chloride induced corrosion is a key obstacle in KMEs goal of reaching a steam temperature of 600°C on wood-fired boilers, since alkali chloride induced corrosion has been identified as a limiting factor in these boilers. One way to potentially overcome this problem is to use corrosion resistant coatings/materials. In the present project superheater samples from a biomass fired boiler have been investigated, thermodynamic calculations and screening experiments have been performed in order to identify a possible corrosion resistant coatings. The most promising system (Ni-Al) has in addition been investigated through lab exposures.

Characterization of TP347HFG superheater samples revealed that the steel was not able to form a protective chromia scale under the superheater service conditions and long exposure times. Instead of protective chromium rich scale an outward grown iron rich oxide with a FeCrNi oxide beneath was formed on all samples. Along grain boundaries extensive attack was observed with both K and Cl present and presumably both being active in the corrosion process. The results from the detailed investigation of field samples were combined with thermodynamic calculations in order to select the most promising coating material. Thermodynamic evaluations using Thermo-Calc and screening experiments were used and the Ni-Al system showed largest potential and specifically the Ni₂Al₃ intermetallic phase that was selected for tests. Aluminised samples were produced at DTU using pack cementation. The aluminising led to formation of a $\sim 30~\mu m$ thick layer of Ni₂Al₃.

The Al-Ni system was in addition investigated and compared with a traditional 18-8 stainless steel (304L) through lab exposures. It shows a large potential to form a protective scale in the alkali chloride environment used in the lab. The results have generated an interest among boiler owners and there are expectations to test the Ni-Al system in boilers. The goal with the project has thereby been fulfilled.

Keywords: Alkali chlorine induced corrosion, corrosion resistant coatings/materials, superheater lifetime

Table of contents

1	Introduction	1
	1.1 Background	
	1.2 Description of the research field	
	1.3 Research task	
	1.4 Goal	
_	-	
2	Investigation of plant exposed sample 2.1 Sample information	es 5
	2.1 Sample information	
	2.3 Summary	
3	Thermodynamic evaluation and scree	ning experiments 13
3	3.1 Ni-Al system	
	3.2 Summary	
4	,	17
4	Aluminising 4.1 Production of samples	— — — — — — — — — — — — — — — — — — —
	4.2 Initial screening experiment	
	4.3 Summary	
5	Laboratory exposures	20
•	5.1 Experimental	_
	5.2 Gravimetry	
	5.3 Microstructure investigations	
	5.3.1 Reference exposures of stainles	s steel21
	5.3.2 Exposures of pure Nickel	24
		28
	5.4 Summary	39
6	Analysis of the results	40
7	Conclusions	44
8	Goal fulfilment	45
9	Suggestions for future research work	46
10	Literature references	47
11	. Publications	50

1 Introduction

1.1 Background

In order to reduce CO_2 emissions, DONG Energy intends to convert PF (pulverised fuel) SC (supercritical) boilers from being fossil-fired (coal or gas) to be wood-fired. Biomass is much more corrosive than fossil fuels, and thus the outlet steam temperature of converted units most likely needs to be lowered in order to obtain acceptable corrosion rates.

In Denmark, extensive research has been performed within straw-fired CHP (combined heat and power) units in order to identify corrosion mechanism, optimum superheater material and optimum steam outlet temperature [1, 2]. Exposures include cooled probes, test superheaters, and test tubes in existing superheaters. These investigations propose that KCl from biomass causes Cl induced corrosion. Exposure of various steels with Cr content varying from 2½ to 30 wt% suggests minimum overall corrosion for steels with a Cr-content between 12 and 18 wt%. The low chromium steels exhibit a high material loss whereas the higher chromium steels are characterized by severe internal corrosion in the form of chromium depletion. DONG Energy considers TP347HFG and similar 18% Cr steels as being the most suitable superheater materials in biomass-fired units.

Protective oxide is formed at metal temperatures below 500°C and the corrosion rate is modest. Between 500 and 520°C either protective oxides or grain boundary attacks are observed, whereas chromium depletion and grain boundary attack always are observed at higher temperature. Significant increase in corrosion rate is observed with increasing temperature. It is possible to reach an outlet steam temperature of 540°C in a well-designed straw-fired unit and still have acceptable corrosion rates.

Wood contains much less KCl than straw and is thus considered a less corrosive fuel. However, investigations of superheater tubes from wood-chip fired CHP boilers have shown that KCl is deposited on part of the superheater leading to chlorine induced corrosion. On such locations, corrosion morphologies and corrosion rates were comparable to those observed during straw-firing. In addition, aerosol measurements at a PF-SC unit during wood-pellet and gas firing showed the presence of significant amount of KCl aerosols. Thus, chlorine induced corrosion is expected locally on superheaters during wood-firing in PF-SC boilers.

Experiences from straw-fired units suggest unacceptable corrosion rates at outlet steam temperatures above 540°C even for superheaters fabricated in the optimum 18% Cr steels. Thus, DONG Energy believes that coating the superheater with corrosion resistant material is needed in order to achieve higher outlet steam temperatures. Commercial available protective coats are mostly variations of Alloy 625, i.e. they are nickel based materials which rely on the formation of a protective Cr-rich oxide layer. Since selective corrosion of Cr in steel is observed during straw-firing, it is doubtful that such coats can be used at steam temperatures higher than 540°C in biomass-fired boilers.

1.2 Description of the research field

The fireside environment in power boilers may be quite corrosive, especially in boilers firing biomass, where the fireside environment is characterized by a combination of high levels of reactive alkali (NaCl and KCl) together with HCl and relatively low SO_2 concentrations.

Several studies report on the corrosive effect of HCl(g) or $Cl_2(g)$ on pure metals [3-7] and alloys [8-20]. Investigations of the effect of HCl and Cl_2 on stainless steel show that the corrosion process is initially very fast. The corrosive action of Cl-containing species at high temperature is usually explained by the so-called "active oxidation" mechanism in which Cl_2 and $MeCl_2$ play a crucial role [5, 6, 8, 10]. Thus, molecular chlorine is supposed to diffuse through the oxide scale to the metal/oxide interface, where it forms volatile transition metal chlorides. The latter compounds are then supposed to diffuse to the scale/gas interface where they decompose, forming oxide and releasing chlorine, which can then continue the reaction.

Recently, the influence of HCl + O_2 on initial stages of corrosion of stainless steel 310S at 500°C was investigated [20]. It was shown that transition metal chlorides form rapidly throughout the scale. With time, the chloride species decompose, leaving a rough scale consisting mainly of $(Fe,Cr)_2O_3$. An electrochemical reaction scheme was proposed for the initial stages of corrosion where HCl is dissociated at the same time as O_2 is reduced on the scale surface, forming chloride ions and water. This reaction is coupled to metal oxidation at the scale/metal interface by electronic current and by grain boundary migration of chloride ions and cations. In contrast to active oxidation, this reaction scheme does not involve the diffusion of Cl_2 , HCl or metal chloride molecules through the scale.

Extensive research about the corrosiveness of alkali chlorides towards low alloyed and stainless steels have been performed at the High Temperature Corrosion center (HTC) at Chalmers [21-23]. In addition to chlorine, it has been proposed that the corrosiveness of KCl on chromia forming steels is caused by the degradation of the protective oxide by the formation of alkali chromates. One way to mitigate the effect of alkali chlorides have been to convert them in to corresponding alkali sulphates, which do not attack the protective chromium rich oxide [24]. This has been successfully evaluated by means of fuel additives in several projects [24-26]. The other opportunity to increase the lifetime of a biomass or waste fired CHP is to change the material, either by coatings or better bulk materials.

1.3 Research task

Severe corrosion is expected to occur locally in wood-fired PF SC boilers, which means that the outlet steam temperature needs to be reduced on converted plants unless more corrosion resistant materials are installed or additives are used. The first aim of this project is to obtain more detailed understanding of the corrosion mechanisms during biomass firing by investigating superheater samples from CHP biomass-fired units with advanced microscopy.

The second aim of this project is to identify and test alternative materials that can provide corrosion protection in biomass-fired boilers at outlet steam temperatures of at least 580°C, i.e. outlet temperatures of PF-SC boilers. Due to the poor corrosion resistance of chromia forming steels and alloys at these temperatures, alloys relying on other oxides as protection are suggested to be included in the project. Possible materials could be silica/MoSi, NiAl, oxides of reactive elements, etc.

Thermodynamic calculations using Thermo-Calc [27] will be performed in order to identify materials, which may provide protection against the corrosion. The most promising materials, according to the calculations, will be exposed in laboratory furnaces at 600° C and compared to reference exposures of un-coated 304L. The materials will be exposed in an O_2 and H_2O mixture without KCl in order to create references, which will then be compared to samples exposes in the presence of KCl. Exposure times up to 168 hours will be used and mass gain will be measured. The corrosion attack of selected samples will be investigated by X-ray diffraction (XRD), light optical microscopy (LOM), scanning electron microscopy (SEM), energy dispersive spectroscopy (EDS), focused ion beam milling (FIB), and transmission electron microscopy (TEM).

The project contributes to the research area in the following ways:

- Increased fundamental understanding of the corrosion phenomena in biomass fired power plants through detailed characterization of superheater samples
- Identification of a candidate material through thermodynamic considerations
- Testing of the candidate material in a controlled laboratory setup in an O₂ and H₂O mixture with KCl and also without KCl to create references.

1.4 Goal

Severe corrosion is expected to occur locally in wood-fired PF SC boilers, which means that the outlet steam temperature needs to be reduced on converted plants unless more corrosion resistant materials are installed or additives are used. The overall goal of the present project is to identify a possible material for superheater tubes, which allows an outlet steam temperature of at least 580°C on biomass converted fossil-fired units. This goal is in line with the overall KME goal to verify an increase of the steam temperature by at least 50°C from approx. 540°C for clean biofuels (wood, forest residue).

1.5 Project organisation

The project is jointly performed by HTC at chalmers and DONG Energy. The following personnel at HTC (Chalmers) participated in the project: Torbjörn Jonsson, Jesper Liske and Andreas Slomian.

From DONG Energy, Anette Nørgaard Hansson and Kristian Vinter Dahl participated in the project. Anette Nørgaard Hansson left DONG Energy in December 2012 and Kristian Vinter Dahl left DONG Energy in February 2013. In September 2013 DONG Energy engaged an agreement with the Technical University of Denmark (DTU) for the remainder of the work period allowing Kristian Vinter Dahl, now at DTU, and Ph. D student Saeed Kiamehr and Post Doc Trine Nybo Lomholt to participate in the project.

Project leader was Torbjörn Jonsson, HTC.

The roles of partners are listed in Table 1.

Table 1: Role of partners in the project.

Part Participants role in the project							
DONG Energy	Thermodynamic calculations in order to identify possible material solutions and investigation of superheater samples by advanced microscopy						
	Supplying material for testing, including production of coated samples.						
Chalmers/HTC	Responsible for laboratory exposures, analysis and corrosion evaluation						

The members of the reference group were:

Annika Stålenheim: Vattenfall Research & Development

Guocai Chai: AB Sandvik Materials

Mats Åbjörnsson: E.ON Värme Sverige AB

Søren Aakjær Jensen FORCE Technology (Member since November 2013).

The project was financed within the frame work of KME by the Swedish Energy Agency. The total project budget was 1733 kSEK.

2 Investigation of plant exposed samples

2.1 Sample information

The plant exposed samples were available from superheater test sections at Amagerværket in Copenhagen through collaboration with Vattenfall. At the time of the plant exposures, Amagerværket was still owned by Vattenfall but is as of 1. January 2014 owned by HOFOR (Hovedstadsområdets Forsyningsselskab). Amagerværket consists of 2 operational units that produce both heat and power. Amagerværket unit 1 was first operational in 1971 as a coal-fired unit but has since 2004 undergone an extensive renovation to a multifuel suspension-fired unit with biomass as the predominant fuel (mix of straw and wood pellets), however coal and oil can also be utilised. The boiler has steam data of 560°C and 18 MPa pressure but when fuelled with biomass the outlet temperature is limited to 540°C to avoid the excessive corrosion observed at higher temperatures [1, 2]. The unit has a capacity of 68 MW electricity and 250 MJ/s heat.

Test sections were built into the final superheater HT-2 in connection with the renovation. Test tubes were built into banks 13 and 20 in the middle of the boiler at locations of the maximum steam temperature and maximum heat flux. The test sections were welded in as received condition (not machined) in this way there is no influence of deformation on corrosion rates.

The tubes available for the present investigation were made in TP347HFG material (18Cr-10Ni-Nb), see chemical composition in Table 2. The tubes were exposed for 5900 hours at a steam temperature of 535° C.

Table 2: Chemical composition of TP347HFG (Vd TÜV547 12.2009)

[wt-%]	С	Si	Mn	Р	S	Cr	Ni	Nb+Ta
min.	0.06	-	ı	-	ı	17.0	9.0	8xC
max.	0.10	0.75	2.0	0.040	0.03	20.0	13.0	1.0

Scanning electron microscopy (SEM, JEOL-5900) was done on polished crosssections prepared without the use of water to not wash away corrosion products. Transmission electron microscopy (TEM, FEG-TEM, JEOL 3000F) was performed on a thin foil prepared by focussed ion beam milling and subsequent lift out. Chemical mapping using energy filtered TEM (EFTEM) was used to investigate the distribution of chemical elements, e.g. O, S, CI, Fe, Ni etc. on a very local scale within the oxide.

2.2 Results

Figure 1 shows an SEM image of the corrosion attack on TP347HFG exposed at a steam temperature of 535°C, which is very near to the present upper acceptable temperature limit, which is 540°C.

A thick layer of deposits and oxides is found at the outer surface. EDX reveals that the deposit is rich in K, Ca and S. It is assumed to be primarily K_2SO4 and $CaSO_4$. The oxide is iron-based. Outwards and inwards growing oxide layers are found closer to the steel, the outwards growing oxide layer is primarily iron rich, while the inwards growing layer is a mixed Fe-Cr(-Ni) oxide.

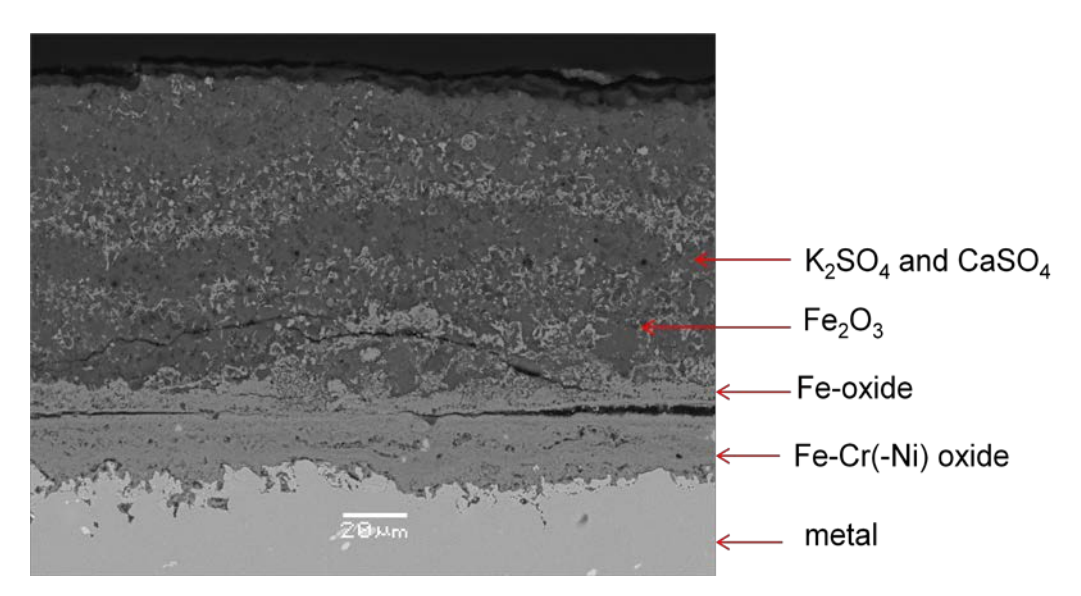
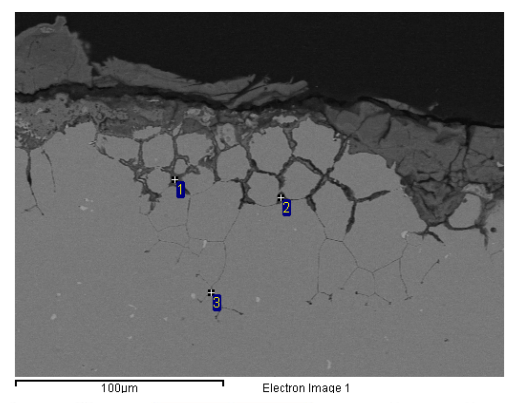


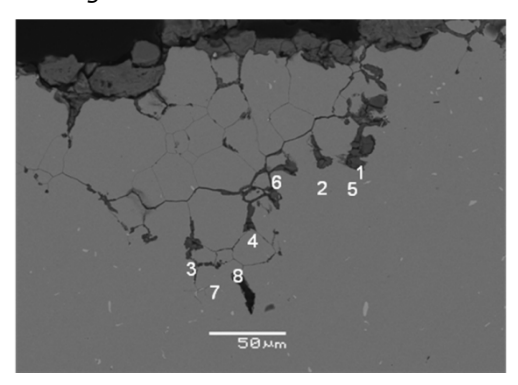
Figure 1: Deposit and oxides formed on TP347HFG after 5900 hours of service. Backscatter electron (BSE) contrast image.

At many locations, extensive attack can be observed along grain boundaries. Corrosion products containing both Cl and K and also some S can be identified in the grain boundaries. Two locations with corresponding EDX measurement results are shown in Figure 2 and Figure 3. The corrosion products lying above the zone of grain boundary attack are rich in S and are highly inhomogeneous with some areas rich in Ni and others rich in Cr, see Figure 4.



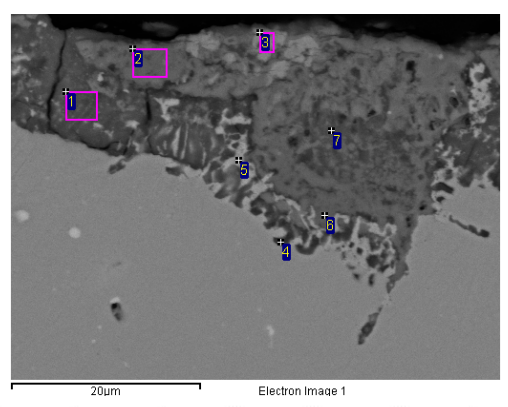
Spectrum	0	Si	S	CI	K	Cr	Mn	Fe	Ni	Nb
1	17.2	1.7		2.3	4.0	30.7		20.3	9.2	14.7
2	17.6	1.3	1.1	3.6	2.7	45.5		23.0	5.2	
3	0.6					23.9	1.5	64.6	9.4	

Figure 2: Extensive attack along grain boundaries, K and Cl are located in the boundaries. BSE contrast image.



Spectrum	0	Si	S	CI	K	Cr	Mn	Fe	Ni	Nb
1	25.0	0.8	0.5	8.0	1.5	45.2		14.3	4.8	
2	20.2	0.9		8.1	1.3	31.9		31.8	5.7	
3	22.3	1.1	1.1	8.9	1.9	42.6		18.4	3.8	
4	18.9	1.2	0.5	7.1	1.3	39.4		25.2	6.5	
5	27.3	1.5	1.0	8.5	1.5	45.2		7.6	5.8	1.8
6	12.1	1.6	0.4	7.2	1.2	36.8	1.6	31.9	5.8	1.4
7	3.5		0.6	2.8	0.8	45.8	3.0	37.6	5.9	
8	5.5	0.5	0.4	2.7	0.4	29.7	1.7	49.2	9.8	

Figure 3: Extensive attack along grain boundaries, K and Cl are located in the boundaries. BSE contrast image.



Spectrum	0	Si	S	CI	K	Cr	Mn	Fe	Ni	Nb
1	19.9	1.6	6.0	1.2	1.4	12.1		23.4	34.5	
2	15.1	1.0	5.9	0.6		59.2		14.0	4.3	
3	3.8	0	23.8			4.2		4.2	64.0	
4	7.8	1.7	0.8		1.1	17.5	1.4	48.1	20.4	1.2
5	3.1	0.5	2.2		0.2	11.4		36.3	46.3	
6	14.9	0.8	7.0			63.0		8.3	6.0	
7	14.8	1.1	10.6		1.2	22.4		28.3	21.4	

Figure 4: Highly inhomogeneous corrosion products are formed above the zone of internal grain boundary attack. Generally these corrosion products are enriched in S with local Ni or Cr rich areas. BSE contrast image.

A thin foil for TEM was prepared using focussed ion beam (FIB) and subsequent lift out from the location shown in Figure 5. The thin foil spanned from the outer oxide/corrosion products across the interface to the metal and into the zone with internal grain boundary attack.

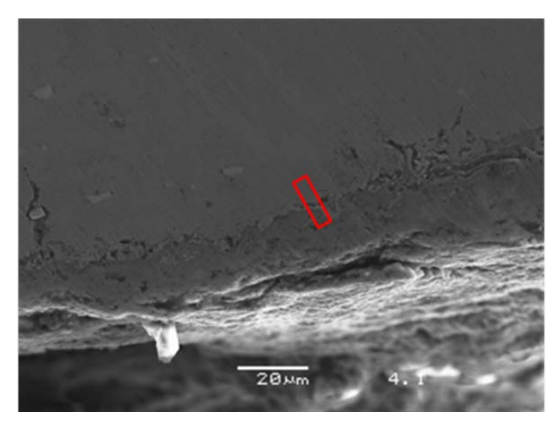


Figure 5: Location of TEM sample.

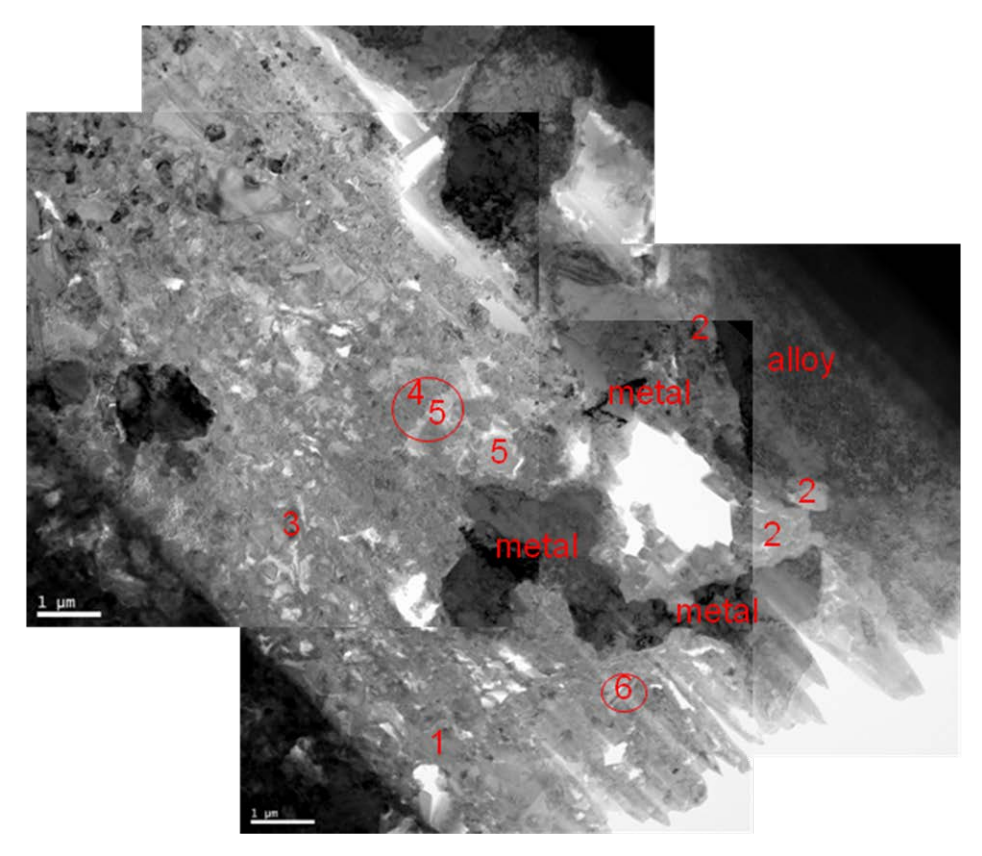


Figure 6: TEM thin foil showing an inhomogeneous oxide/corrosion product layer that still contains some metallic parts, the bulk alloy starts in the upper right hand part of the picture.

1) high S (Fe,Cr); 2) Fe-Cr oxide; 3) Contains Ni and P; 4) high Cr + S + O; 5) high Fe + S + O; 6) high Fe + S + Cl.

The metal parts in the layer are typically depleted in Cr and enriched in Ni (Cr: 6 Fe: 57 Ni: 37) compared to the original alloy composition.

The rings indicate positions where chemical mapping by EFTEM was applied.

Close to the interface towards the alloy, EDX measurements shown in Figure 6 indicate the presence of an Fe-Cr rich oxide. The outer part of the layer is a highly inhomogeneous mix of different corrosion products and metallic parts.

Chemical mapping using EFTEM was used to see the local distribution of chemical elements. Examples are shown in Figure 7 and Figure 8 from the locations marked 6 and 4 in Figure 6. A high intensity indicates presence of the element, but careful interpretation should be done where the foil is very thin (bright areas in the bright field TEM image), since artefacts may be present at these locations.

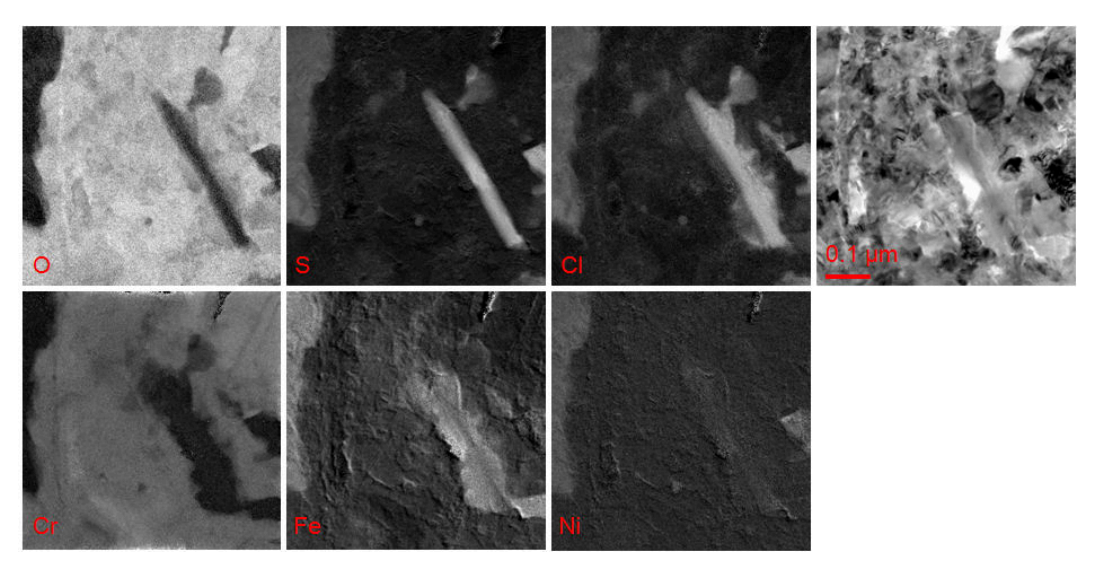


Figure 7: Chemical maps obtained using EFTEM and corresponding TEM bright field image. Location 6 in Figure 6.

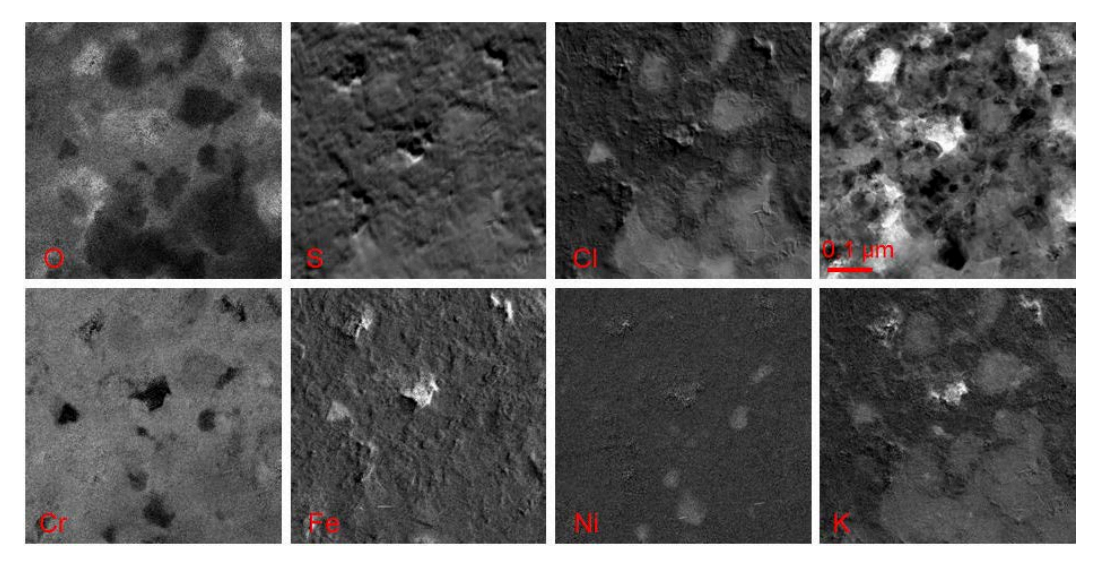


Figure 8: Chemical maps obtained using EFTEM and corresponding TEM bright field image. Location 4 in Figure 6.

The investigations reveal that the corrosion layer is inhomogeneous on a nano-scale and further the following observations can be made:

- Fe and not Cr is observed together with Cl
- NiS particles are formed
- S and Cl are observed together
- K and Cl are observed together
- S, Cl and O are not observed together

TEM EDX in the vicinity of a grain boundary just below the outer corrosion layer showed primarily S-rich corrosion products; see Table 3, as well as Crdepletion inside a single grain, EDX analysis 9-12 in Figure 9 and Table 3.

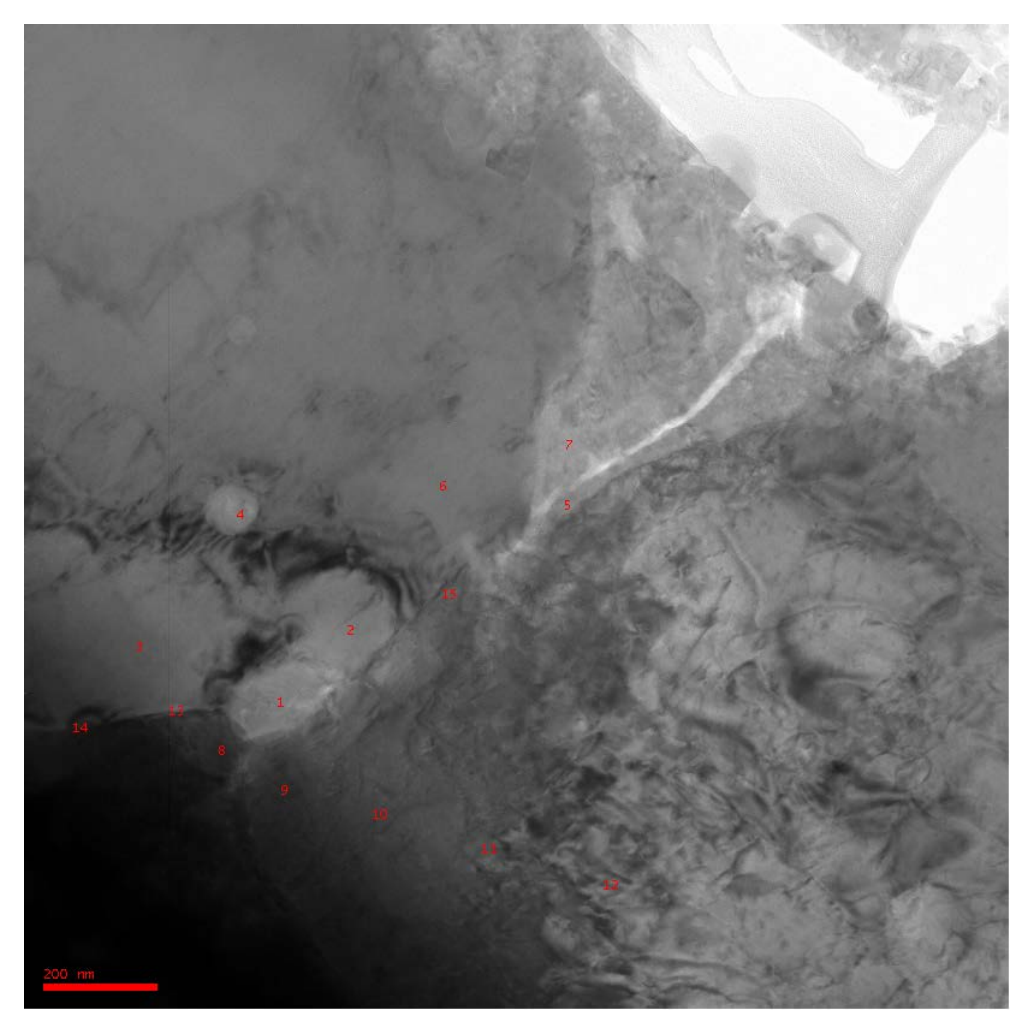


Figure 9: TEM brightfield image of a grain boundary below the outer oxide layer.

Table 3: TEM EDX Composition measurements for measurement locations shown in **Figure 6**.

		0:		01			_			
analysis	0	Si	S	CI	Cr	Mn	Fe	Ni	Nb	Мо
5	17.5	1	15.6		22	0.7	24.1	1.7	2.8	14.5
7	17.1	0.4	9.7	0.5	31.7	1.2	32.2	6.3	0.9	
1	15.6	1.1	13.6		21.6	8.0	27.8	1.9	2.1	15.5
2	3.9				14.4	0.7	45.4	35.6		
4			16		4.9	24.1	34.8	20.2		
13	6.8	4.5	0.5		10.3	0.6	44.4	32.9		
6					2.9		55.9	41.2		
15					5.7		52.6	41.7		
8					10.7	0.5	50.4	38.2		0.3
9					2.5		41.3	56.2		
10					3.4		59.5	37.1		
11					5.9		61.2	32.9		
12					5.9		61.2	32.9		
14					7.8		50.8	41.4		
3					2.9		45.9	51.2		

2.3 Summary

From the investigations it is clear that the TP347HFG material is not able to form a protective chromia scale under the present superheater service conditions and long exposure times. Extensive attack is found along grain boundaries with both K and Cl present in the boundaries and presumably both being active in the corrosion process.

Transmission electron investigations reveal that the formed oxide is inhomogeneous on a nanoscale, and consists of a mixture of oxides, metallic regions depleted in Cr and enriched in Ni and mixed corrosion products containing either Cl or S or both. Interestingly Fe and not Cr were observed together with Cl in the two EFTEM locations, but this trend needs further investigation. Underneath the oxide scale, corrosion products are found in grain boundaries and significant chromium depletion is found.

The interpretation of the corrosion attack is complex due to the simultaneous presence of several degradation mechanisms. It is clear that also S and not only K and Cl could be found in the complex corrosion products after breakdown of the protective scale. It is however believed that the initial reaction between potassium and chromia oxide to form potassium chromate is the main reason for the TP347HFG steel not being able to form a protective oxide under the service conditions [21-23]. Therefore the first step in identifying candidate materials solutions should be to evaluate the resistance against KCl and thereafter the other corrosive species in the environment. The repeated SEM-EDX findings of K and Cl in the grain boundaries at the internal corrosion front underline the importance of the resistance versus KCl.

3 Thermodynamic evaluation and screening experiments

(Work by Ph. D. Student Saeed Baghsheikhi as part of the DTU Green project)

Simultaneous with the investigations on samples from plant exposed superheater tubes, thermodynamic calculations have been performed in order to identify materials with low reactivity towards KCI.

Thermo-Calc version S [27] with the databases TCFE and SSUB was used to screen the thermodynamics of $M-O_2-Cl_2$ systems at 600°C in order to select candidate oxide formers that have a large oxide stability area (transforms from oxide to chloride at a high Cl_2 partial pressure) and candidate matrix materials, which have a large metallic stability area (transforms from metal to chloride at a high Cl_2 partial pressure), see Figure 10.

Based on this approach a list of materials was selected (listed in no special order):

Oxide formers: Al, Si, Hf, Zr, Ti, Cr, Ce, Fe, Mn, Y, Ta.

Matrix materials: Mo, Ni, Co.

It is already known and also supported from the present investigations of exposed superheater samples that chromia is not protective when firing with biomass. This is likely to be related to the breakdown of chromia through reaction with potassium [21-23]. Therefore a screening of suitable oxides must also incorporate the affinity towards potassium as a necessary criterion. Unfortunately only limited thermodynamic data is available for such a screening. Thus due to uncertainty about the accuracy of the thermodynamic data that could be found and also the complete lack of data for many oxides, screening experiments were done.

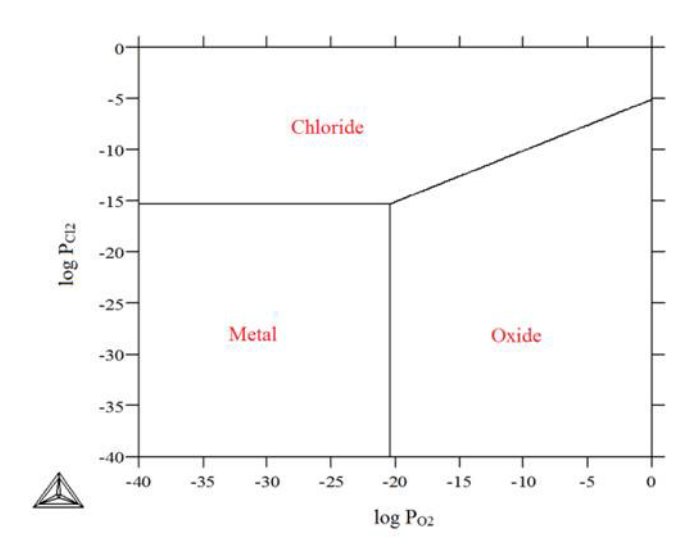


Figure 10: Schematic stability diagram for an $M-O_2-Cl_2$ system at constant T.

Oxides on powder form were mixed with KCl and pressed into pellets like the one shown in Figure 11.



Figure 11: Pellet consisting of a mixture of KCl and oxide.

Pellets were made from mixtures of KCl and the following oxides:

 ZrO_2 , TiO_2 , Y_2O_3 , SiO_2 , Ta_2O_5 , Cr_2O_3 , HfO_2 , CeO_2 , Al_2O_3 , Fe_2O_3 , Mn_3O_4 , NiO_3O_4

The pellets were then exposed to an environment mimicking that of biomass firing: 5% $O_2(g)$ + 15% $H_2O(g)$ + $N_2(g)$ at 650° C for 15 hours. The temperature was increased 50° C compared to the calculations in order to accelerate reactions. Because of the relatively short testing times possible in the lab, this was used as a means to accelerate tests.

X-ray diffraction (XRD) was used before and after exposures to document the presence of reaction products. Figure 12 shows the measured spectra for Cr_2O_3 and clearly shows that potassium-chromate has formed during the exposure.

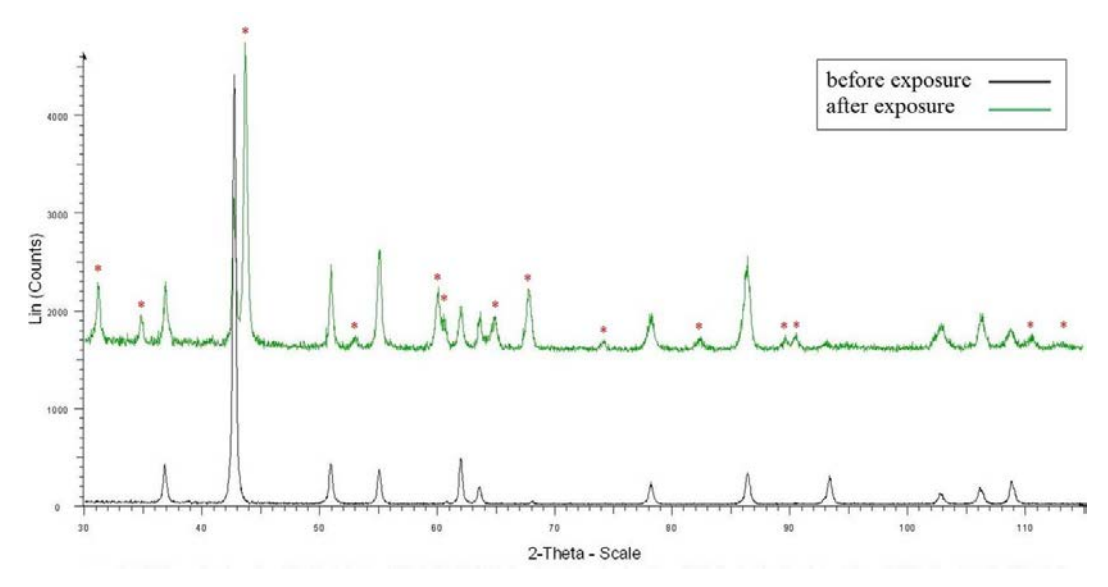


Figure 12: XRD spectra of the pellet consisting of Cr_2O_3 and KCl, before and after exposure. The new peaks (marked with stars) that appear after exposure are due to the formation of K_2CrO_4 .

XRD was performed on all samples and in summary documents that the following oxides do not show any measurable reactivity (listed in no special order):

 Al_2O_3 , NiO, Co_3O_4 , TiO_2 (anatase & rutile), ZrO_2 , CeO_2 , Fe_2O_3 , HfO_2 , Y_2O_3 , Ta_2O_5 While reactivity is clearly seen for Cr_2O_3 and some further investigations are needed for SiO_2 and Mn_3O_4 .

3.1 Ni-Al system

Based on the above considerations the Ni-Al system was a natural choice for further studies. The aluminium system is interesting because alumina already has shown some promise of protective behaviour on preoxidised FeCrAl alloys [28, 29] and aluminium rich coatings are widely used in e.g. the gas turbine industry because of the protective and slow growing nature of the Al_2O_3 oxide, albeit at higher temperatures [30]. Tests of the β -NiAl intermetallic phase has shown less corrosion attack than iron based compositions under KCl-NaCl induced corrosion at 670°C [31]. Several of the other identified oxides cannot be expected to be protective or slow growing and some will also result in significantly more expensive solutions than an alumina-former. In future work additions of trace amounts of some of the elements, e.g. Ce, Hf and Y could be of interest, since such additions have proven positive effects on the formation and protective behaviour of alumina oxide [32].

The stability diagrams for $Ni-O_2-Cl_2$ and $Al-O_2-Cl_2$ are shown in Figure 13. For Ni there is a large metallic stability area, while Al has a large oxide stability area

In the present project it was decided to test the Al-rich Ni₂Al₃ intermetallic phase, since the formation of a protective oxide could benefit from the higher

Al-content compared to the β -NiAl phase tested in [31]. The Ni₂Al₃ phase has very fast growth kinetics compared to the other Ni-Al intermetallic phases, this is attractive due to shorter coating/processing time and/or possibility for using lower processing temperatures [33, 34]. The fast diffusivity of Al in the phase could also help in formation and self-healing of the protective oxide.

Figure 14 shows a Ni-Al-O₂-Cl₂ stability diagram for the Ni_2Al_3 intermetallic phase. Interestingly the area of metal stability for the Ni_2Al_3 phase is larger compared to the pure aluminium.

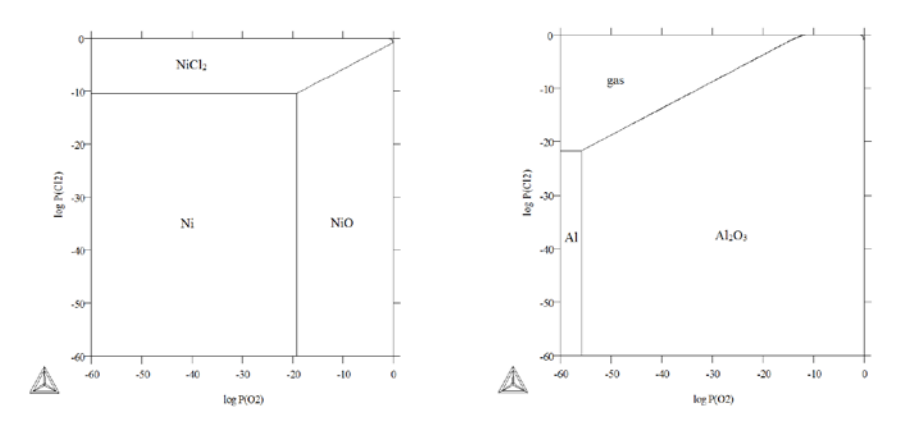


Figure 13: Stability diagrams for Ni-O₂-Cl₂ and Al-O₂-Cl₂ systems at 600°C.

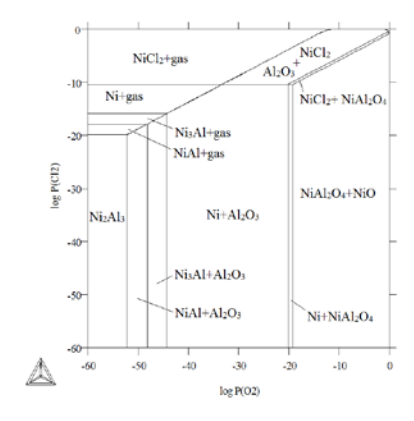


Figure 14: Stability diagram for Ni₂Al₃ at 600°C.

3.2 Summary

A number of candidate alloying systems were identified based on calculated M-O₂-Cl₂ diagrams and screening experiments in an environment mimicking that of biomass firing that tested interaction of oxides with KCl. It was confirmed that chromia was unsuited as protective oxide, due to the interaction with K and formation of K_2CrO_4 . No interaction with Al₂O₃ was observable and therefore based on these results the Ni-Al system and specifically the Ni₂Al₃ intermetallic phase was chosen for the laboratory tests. Nickel was chosen as matrix material due to the large metal stability area in the calculated Ni-O₂-Cl₂ diagrams.

4 Aluminising

Aluminising of Ni-samples was done at DTU using pack cementation. Pack cementation is a standard method for aluminising and is widely applied for gas turbine applications [30]. It can be used on large components with the limit being the size of the furnace equipment. Other processes may be considered for actual tube/boiler manufacturing but pack cementation is well suited for the present testing of the chemical response of the Ni_2AI_3 phase, since high quality uniform coatings can be manufactured in lab-scale equipment. The component to be treated is typically packed in a powder containing an aluminium source and a halide activator. At the process temperature the activator reacts with the aluminium source forming volatile Al-halide compounds that are transported to the sample surface where they decompose releasing Al to diffuse into the component. The process can be carried out at low temperatures limiting changes to bulk microstructure [34].

4.1 Production of samples

Pack cementation of Ni-samples (99.99+% purity) was done out in a tube furnace with an argon protective atmosphere. The pack mixture consisted of 10 wt.% aluminium powder (99.9% purity, max particle size 60μ m), 84 wt.% Al_2O_3 -filler and 6 wt.% anhydrous $AlCl_3$. Powders for the pack were weighed and mixed thoroughly. The pack powder and samples were packed into Al_2O_3 -containers that were then inserted in the tube furnace. The pack was heated to 650° C using a heating rate of approximately 10° C/min, held for 8 hours and then after the treatment cooled to room temperature inside the furnace in argon flow.

Samples were half-circle shaped with a radius of 12.5 mm and a thickness of 2 mm. Prior to aluminising the sample surfaces were ground on SiC paper with grit sizes #320, #500 and #1000 and then thoroughly cleaned in ethanol.

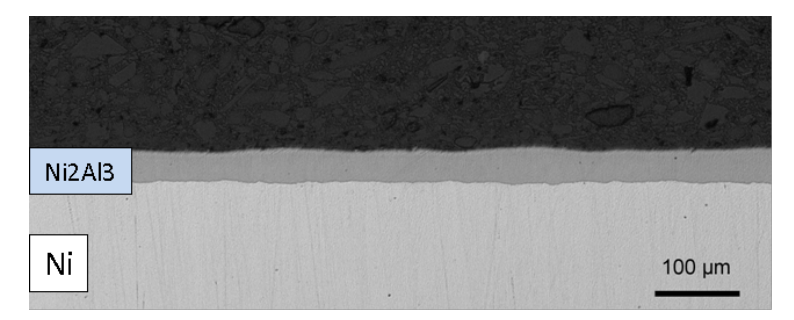


Figure 15: Light optical image of the layer formed after aluminising at 650°C for 8 hours.

The treatment led to formation of a $\sim 30~\mu m$ thick layer of Ni₂Al₃ as shown in Figure 15. The presence of Ni₂Al₃ was confirmed by XRD; see Figure 16. A thin

zone is present between the Ni₂Al₃ layer and the bulk nickel. Phases that may form according to the phase diagram are NiAl, Ni₅Al₃ and Ni₃Al. NiAl has the fastest growth kinetics of these three phases [32] and therefore the thin zone is expected to primarily consist of NiAl.

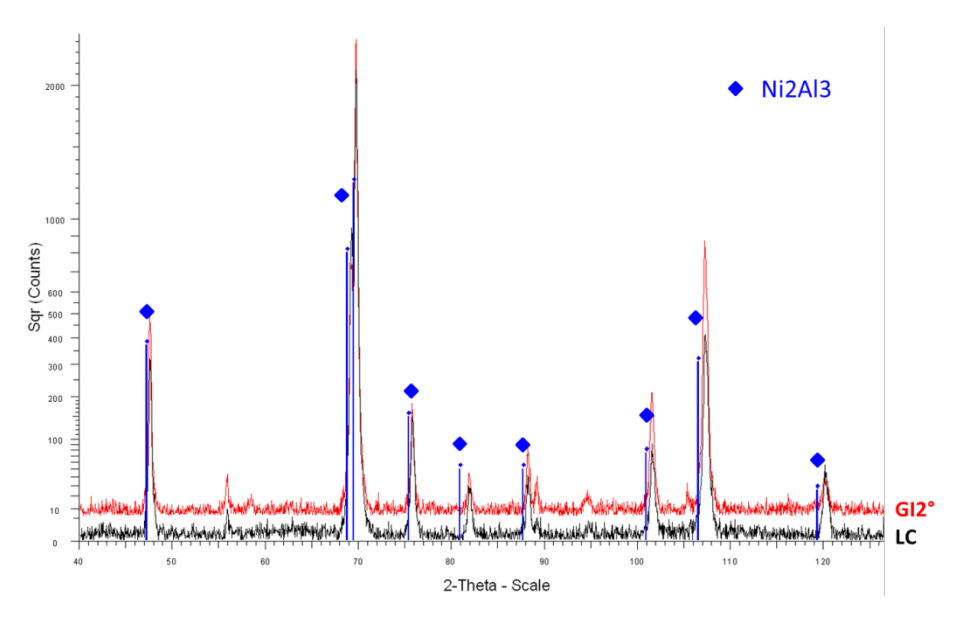


Figure 16: XRD spectra of aluminised sample.

After aluminising the surface of treated samples is generally of a high quality, but in smaller regions some dark staining was visible. It is likely that this staining could be reduced by using a pack containing lower amounts of the aggressive activator. After aluminising the samples were ground using #4000 grit SiC paper and then polished using 3 μm diamond suspension and finally 1 μm diamond suspension.

4.2 Initial screening experiment

An initial screening experiment was carried out at DTU. An aluminised sample was exposed at 600° C for one week in static laboratory air after application of approximately 1 mm of KCl powder to one surface (KCl powder particle size of 63-90µm). After exposure little or no observable surface degradation was visible, see Figure 17. At the interface between bulk nickel and the coating, the NiAl zone has grown as a result of interdiffusion.

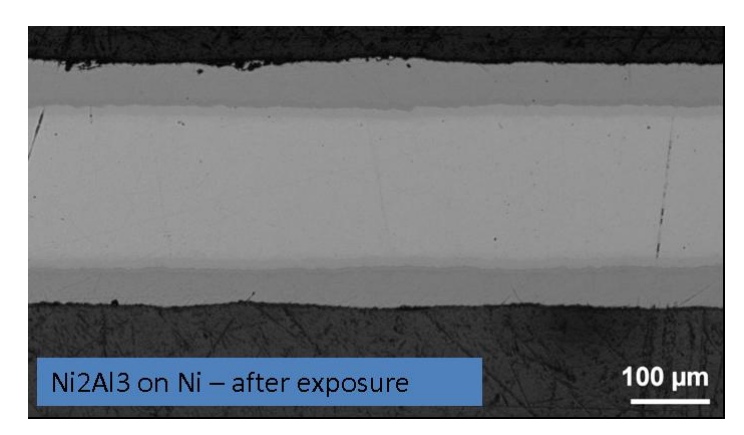


Figure 17: Light optical image of an aluminised sample after KCl exposure at 600°C for one week.

4.3 Summary

Aluminised samples were produced at DTU using pack cementation. The aluminising led to formation of a $\sim\!30~\mu m$ thick layer of Ni_2Al_3 . An aluminised sample was exposed at $600\,^{\circ}C$ for one week in static laboratory air after applying approximately 1 mm of KCl powder on one surface. After exposure little or no surface degradation was observable. At the interface between intermetallics and bulk Ni, the $\beta\text{-NiAl}$ phase had grown due to interdiffusion.

5 Laboratory exposures

Based on the advanced microscopy investigation of field exposed samples and the thermodynamically calculation described above the Ni-Al system was selected for further studies as described above. Both pure Ni and Ni₂Al₃ were investigated through laboratory exposures and advanced microscopy. As a reference the stainless steel 304L was investigated in order to better understand the field samples and to rank the performance of the Ni-Al materials.

5.1 Experimental

In order to prepare the samples for exposure the steel and Ni samples were first mounted on a sample holder and wet ground with SiC paper with increasing grit sizes: #80, #220, #320 and #1000 grits were used. The samples were subsequently polished with 9, 3 and 1 μm diamond size polishing paper whilst lubricated. The samples were rinsed with ethanol (99,5%) in between every grinding and polishing stage. After grinding, glue residue on the sample was removed using cotton pads and acetone, and the samples were cleaned an ultrasonic bath with acetone followed by ethanol. The samples were dried in cool air, checked for imperfections, weighed in a Sartorius R 160 P scale and stored in a desiccator. The aluminising of Ni_2Al_3 coated samples was described in section 4.1. After aluminising the samples were ground by hand with SiC paper grit size #4000 and polished with 3 and 1 μm diamond suspension.

KCl was applied to the samples by spraying a saturated solution of KCl in a 20:80 mixture of water and ethanol (99,5%) while continuously drying the sample with heated air prior to exposure. The desired degree of KCl surface coverage was 0,10 mg/cm². All samples were exposed at 600 °C in an environment containing 5% O_2 , 40% H_2O and 55% N_2 in an electrically heated tube furnace with a gas flow of 1000 mL/min. The samples were exposed for 1, 24 and 168 hours, both with and without KCl. After exposure, the samples were allowed to air cool followed by weighing. The exposed samples were examined in a FEI Quanta 200 FEG ESEM equipped with an Oxford Inca 300 EDX system for chemical analysis in high vacuum mode. X-ray diffraction was performed in a Siemens D5000 Powder Diffractometer. Transmission electron microscopy was performed using a JEOL 3000F FEG-TEM. Thin foils were produced in an FEI Quanta 200 3D SEM. Broad ion beam sections were produced in Leica Broad ion beam (BIB) workstation.

5.2 Gravimetry

The corrosiveness of small amounts of KCl towards 304L, Ni and Ni₂Al₃ is illustrated in Figure 18 showing the mass gain in 5% O₂ with 40% H₂O with and without KCl(s) at 600 °C. In the presence of KCl the initial corrosion rate is strongly accelerated for the stainless steel. In the absence of KCl the stainless steel shows a non-protective behaviour after longer exposure times

due to evaporation of CrO₂(OH)₂ in the presence of water vapour [33]. Both Ni without KCl and with KCl show a similar behaviour as the stainless steel in the presence of KCI, i.e. after breakaway corrosion. However the presence of small amounts of KCl does not result in a faster corrosion rate of Ni. Instead both the Ni without and Ni exposed in the presence of KCl follow a similar growth rate. KCl is known to evaporate under these conditions [21], which could explain the smaller mass gain of Ni exposed with KCl. The mass gain of the Ni sample exposed for 168 hours corresponds to a calculated oxide thickness of about 2 µm using NiO. Exposure of the Ni₂Al₃ coated sample indicates the formation of a protective oxide scale with small mass gains. The mass gain of the sample exposed for 168 hours without KCl corresponds to a calculated average oxide thickness of 190 nm, using Al₂O₃. The scatter in mass gain is in addition very small. Exposures of the Ni₂Al₃ coated samples in the presence of KCl gives a mass loss approximately corresponding to the amount of deposited salt. This indicates that very little of the salt reacts with the Ni₂Al₃ phase and that a protective oxide forms also in the presence of KCl similar to the exposure without KCI.

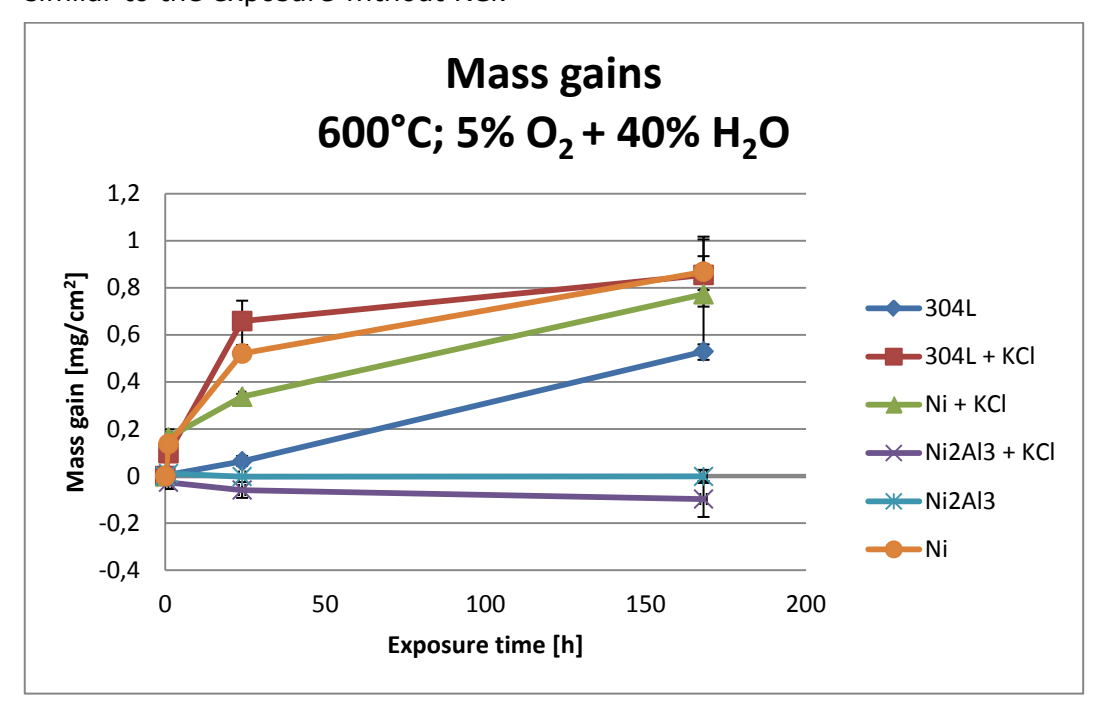


Figure 18: Mass gain of 304L, Ni and Ni₂Al₃ samples exposed with and without small amounts of KCl(s) in 5% O₂ with 40% H₂O at 600 °C.

5.3 Microstructure investigations

5.3.1 Reference exposures of stainless steel

This work has been performed in collaboration with the HTC critical corrosion phenomenon project. Both reference exposures and exposures with KCl have been performed with 304L within the present project. In addition some of the microscopy has been performed while the more detailed microscopy has been

performed within the HTC project. The results of the detailed microscopy are however very important in order to link the field results presented earlier to the lab results in the present project and are therefore included below with references.

The effect of small amounts of KCl(s) (0.10 mg/cm²) on the corrosion behaviour of the austenitic stainless steel 304L (Fe18Cr10Ni) was studied at 600 °C in 5% O_2 + 40% H_2O + N_2 as a reference [21]. KCl was applied by spraying as described above on polished samples, see a SEM plan view image before exposure in Figure 19.

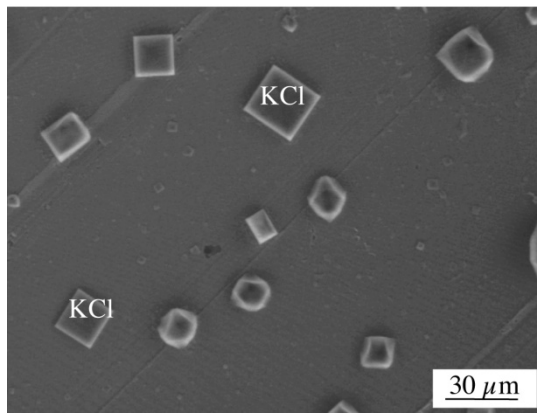


Figure 19: A SEM image of a sample with KCl(s) before exposure.

The mass gain curves, see Figure 18, show the strong effect of small amounts of KCl on the initial corrosion of the 304L stainless steel. Exposures without KCl(s) are included as reference.

The breakdown mechanism of the protective oxide was investigated. This was done through a detailed microstructure characterization of the oxide scales formed after 1, 24 and 168 h. The presence of KCl(s) causes a breakdown of most of the protective scale, even though it is not in direct contact with KCl(s) particles, starting after only 1 h exposure. A fast growing porous oxide formed in direct contact with (former) KCl(s) particles and an about 2 μ m thick scale covered most of the surface. A thin scale covered just some regions after one hour. K_2CrO_4 particles were in addition randomly distributed all over the scale after 1 h exposure, see SEM image in Figure 20.

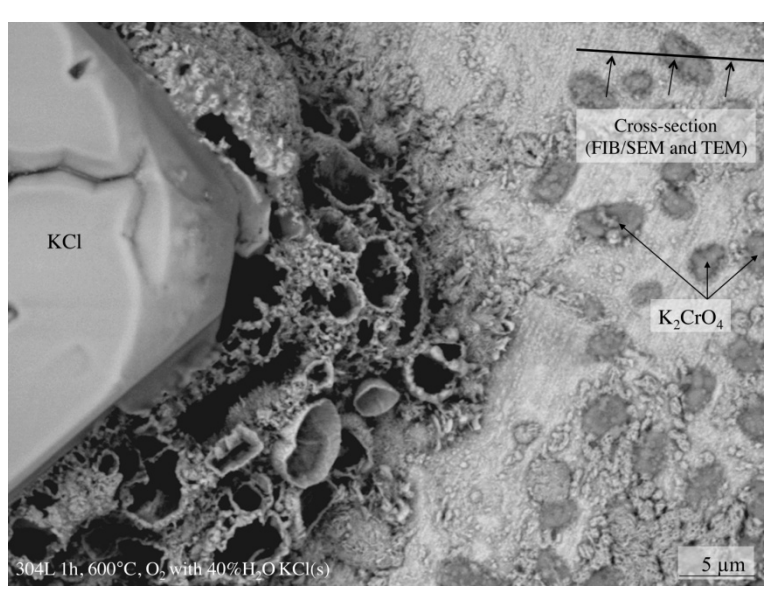


Figure 20: SEM BSE image of 304L samples exposed with KCl(s) at 600 °C for 1h.

The K_2CrO_4 particles are situated above the oxide scale and are not in direct contact with the subjacent metal, see TEM image of FIB cross-section in Figure 21. The thin scale contains lower Cr levels than has been observed in corresponding scales formed in the absence of KCl. The breakdown of the protective scale is suggested to be caused primarily by the formation of K_2CrO_4 , depleting the protective oxide in chromium [21].

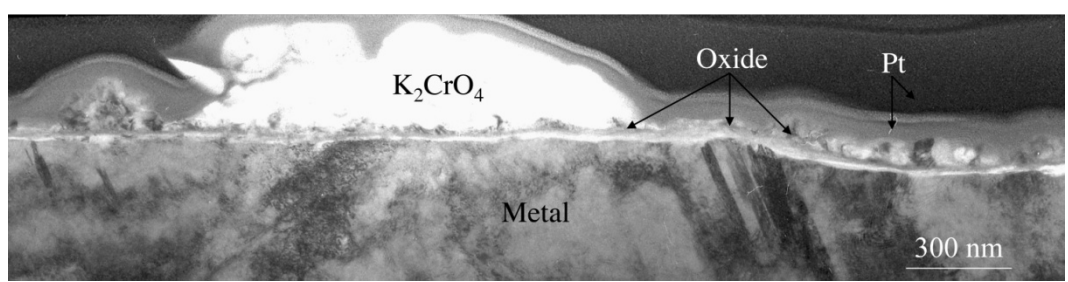


Figure 21: TEM image of samples exposed with KCI(s) at 600 °C for 1h (see position of cross-section in Figure 20).

After one hour of exposure large parts of the sample surface was covered with a thicker scale, see Figure 20. The thicker oxide scale is shown in cross-section in Figure 22. The oxide thickness is generally around 1-2 µm but somewhat thinner just above the steel grain boundary. It is built up by a two-layered structure, *i.e.* an outward growing oxide island and an inward growing oxide crater separated by the original metal surface. Convergent beam electron diffraction (CBED) was employed in the TEM to determine the structure of the oxide scale. It showed that the outer layer has a corundum structure while the inward growing layer has a spinel structure, see CBED patterns in Figure 22. At the interface between the oxide island and the oxide crater several micrometer long horizontal voids can be observed. Another type of pores can also be found, with a diameter typically below 200 nm. A void has formed in the vicinity of the steel grain boundary together with some inward growing oxide.

STEM/EDX analysis showed that the outer layer is Fe rich while the inner layer contains a typical composition of 40 wt.% Fe, 40 wt.% Cr and 20 wt.% Ni. Combining the diffraction analysis with quantitative STEM/EDX analysis shows that the oxide island contains almost pure hematite (Fe $_2$ O $_3$), while the oxide crater contains (Fe,Cr,Ni) $_3$ O $_4$. No or very little (< 0.5 wt.%) K or Cl could be found in the thick oxide scale.

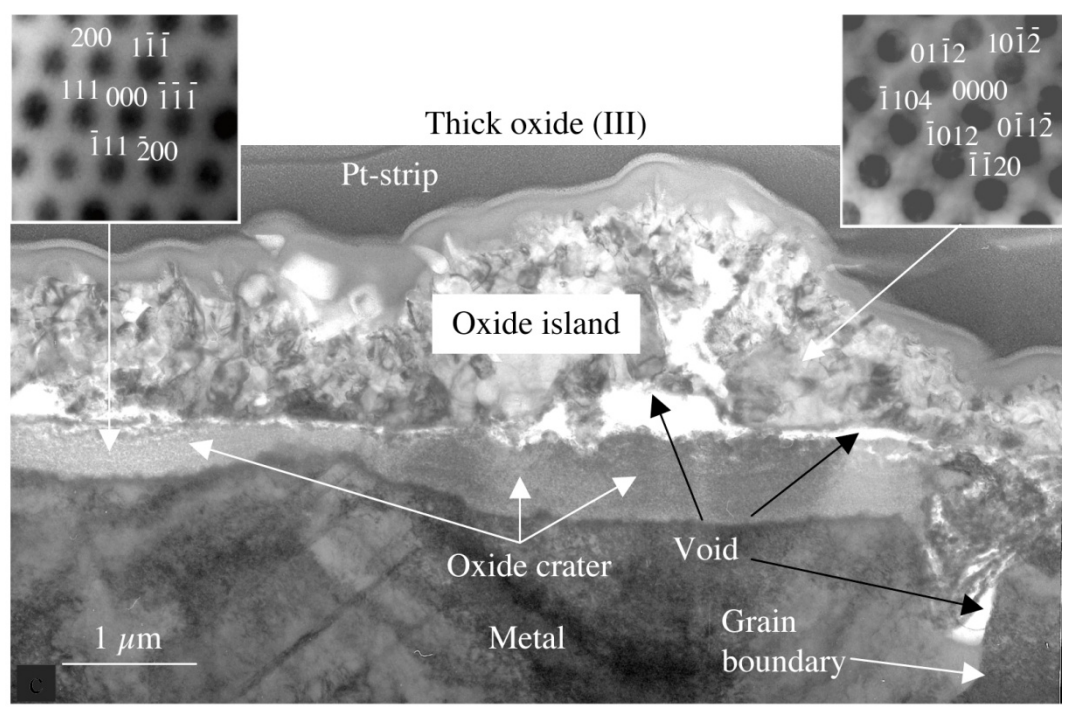


Figure 22: TEM image of the thicker oxide scale formed on samples exposed with KCl(s) at 600 °C for 1h. The thick oxide scale can be divided into an oxide island and an oxide crater. A CBED pattern from the oxide island, indexed a corundum structure (M_2O_3) with the zone axis $\begin{bmatrix} 2 & \bar{2} & 0 & 1 \end{bmatrix}$ and a CBED pattern from the oxide crater indexed as a spinel structure (M_3O_4) with the zone axis $\begin{bmatrix} 0 & \bar{1} & 1 \end{bmatrix}$ are inserted.

5.3.2 Exposures of pure Nickel

In the absence of KCl Nickel shows an approximately parabolic growth rate, see Figure 18. XRD showed the presence of Nickel and NiO after all exposure times indicating a thickness below the penetration depth of the XRD (about 20 μm). After one hour of exposure the sample surface was covered with a smooth oxide scale, see Figure 23. This type of morphology was present after all exposure times (not shown).

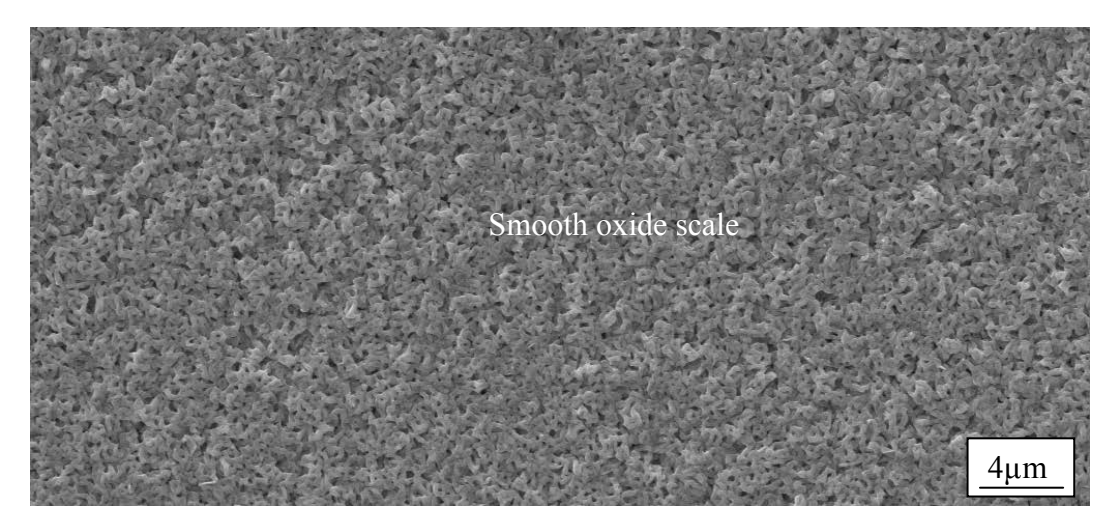


Figure 23: SEM SE image of Ni sample exposed at 600 °C for 1h.

In the presence of KCl the Nickel samples show a smaller mass gain, see Figure 18. This indicates that the growth rate in presence of small amounts of KCl is similar as the reference exposure. The smaller mass gain could be explained by the evaporation of KCl. XRD shows the presence of Ni and NiO on all samples while KCl is detected only after 1 hour of exposure. However, in contrast to the exposures in the absence of KCl, oxidation with KCl(s) gives rise to two different types of morphologies already after 1h exposure, see Figure 24. Thus, the low magnification image in Figure 24 shows a smooth oxide on large parts of the surface while an oxide rim starts to form around KCl particles where KCl particles were deposited prior to the exposure.

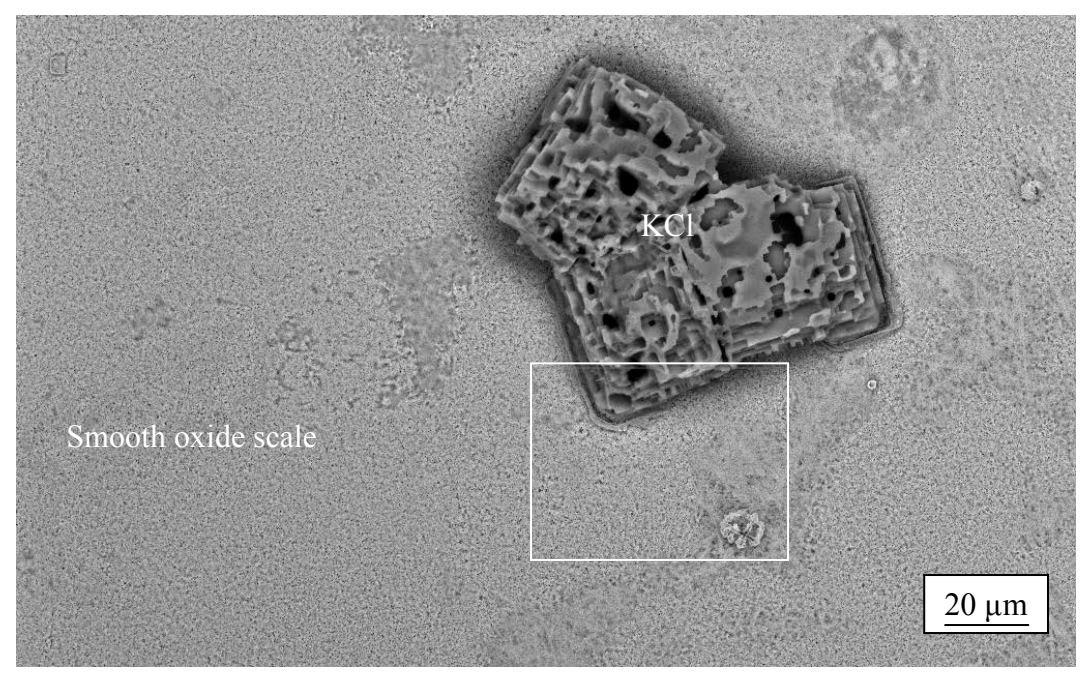


Figure 24: SEM BSE image of the oxide scale and a KCl particle on pure Nickel after one hour of exposure. The main part of the sample is covered with a smooth oxide scale. The marked area corresponds to Figure 25.

The high magnification SE image in Figure 25 shows that an oxide rim has started to grow in the vicinity of the KCl particle. This phenomenon was observed around all KCl particles while the smooth oxide scale in between particles has the same type of morphology as the samples exposed without KCl.

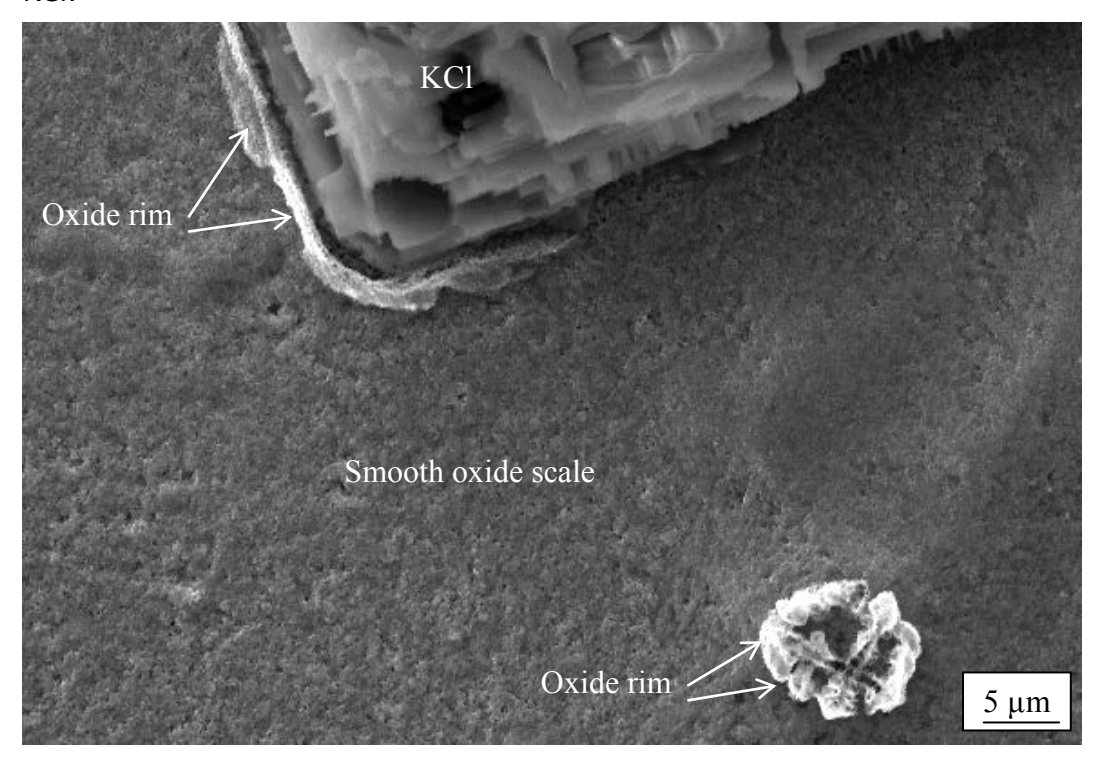


Figure 25: SEM SE image of the oxide scale and a KCl particle on pure Nickel after one hour of exposure, an oxide rim can be seen next to the KCl particle. The main part of the sample is covered with a smooth oxide scale.

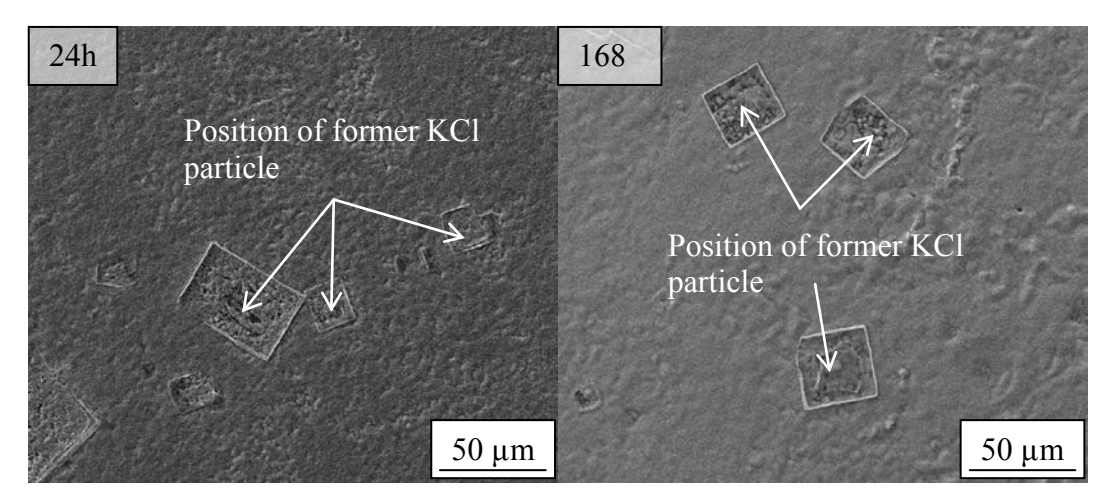


Figure 26: SEM SE images of the oxide scale formed after 24 and 168 hours exposure on Nickel in the presence of KCl. The main part of the sample is covered with at smooth oxide scale while oxide rims have formed around former KCl particles.

After longer exposure times (24 and 168h) most of the KCl has vanished probably due to evaporation leaving only the oxide rims indicating former KCl particles position, see Figure 26. No indication of spallation was observed.

The oxide rims are about 100 nm thick and have a similar height in all rims independent of distribution and particle size of the former KCl particles. In Figure 27 a high magnification image shows the oxide rims after 24 hours exposure.

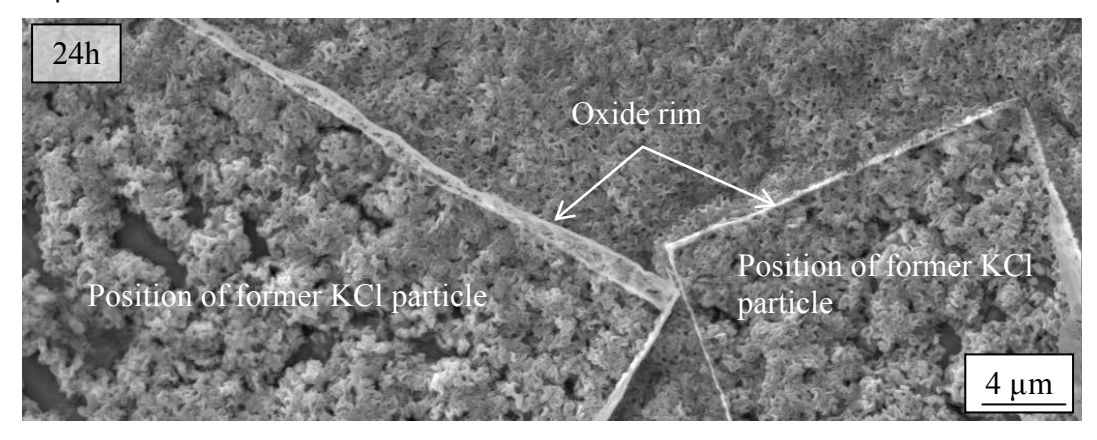


Figure 27: SEM SE image of the oxide scale formed after 24 hours exposure on Nickel in the presence of KCl. The main part of the sample is covered with a smooth oxide scale while oxide rims have formed around former KCl particles.

In some regions of the samples exposed for 168h the oxide rims start to get overgrown, see Figure 28.

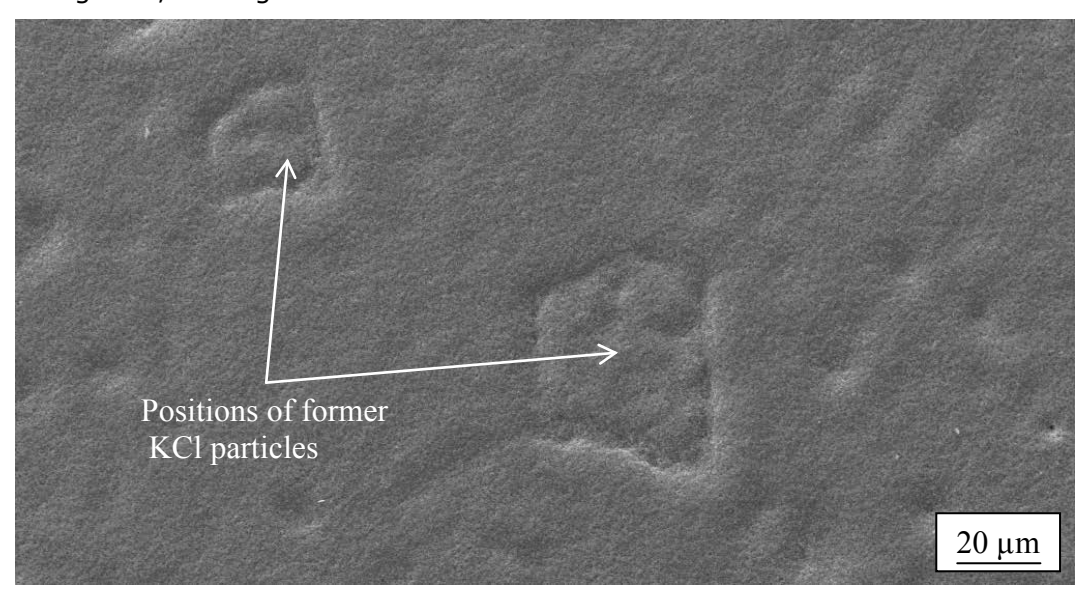


Figure 28: SEM SE image of the oxide scale formed after 168 hours of exposure on Nickel in the presence of KCl. The main part of the sample is covered with a smooth oxide scale and the oxide rims that have formed around former KCl particles are starting to get overgrown.

A BIB cross-section was ion milled through the oxide scale and into the metal on a Nickel sample exposed for 168h in the presence of KCl. In Figure 29 a

SEM BSE images shows one part of the cross-section. The oxide scale was 3-7 um thick in the cross-section and contains many voids. Some of the larger voids could be observed at the metal/oxide interface while the voids tend to be smaller closer to the oxide/gas interface. The oxide grains close to the oxide metal interface are columnar and 300-500 nm wide.

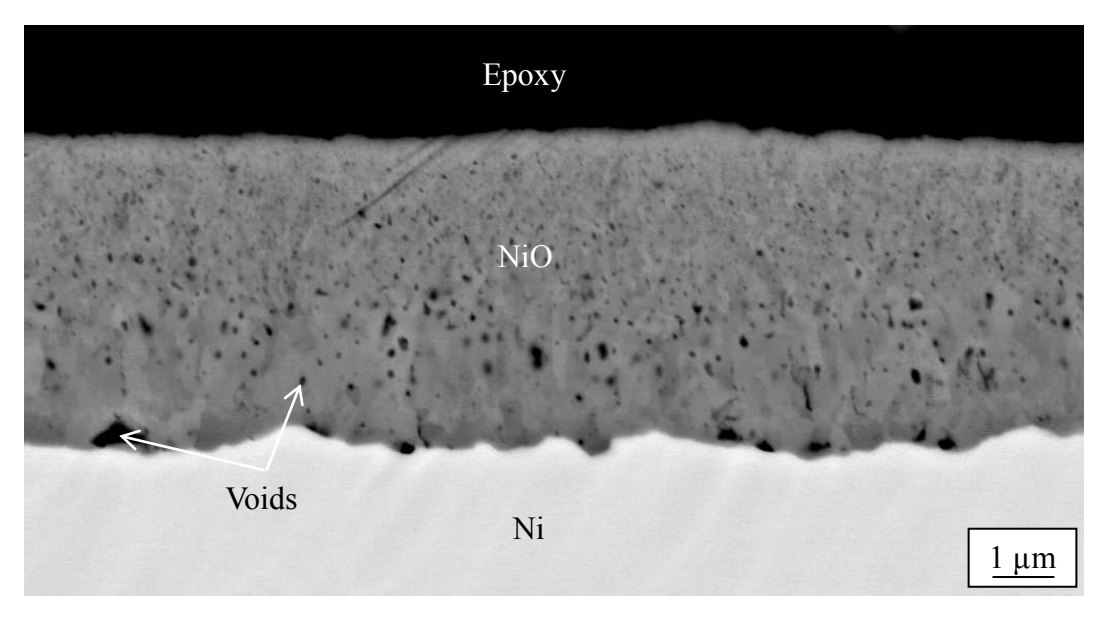


Figure 29: SEM BSE image of an ion milled cross-section of the oxide scale formed after 168 hours exposure on Nickel in the presence of KCl.

5.3.3 Exposures of Ni₂Al₃

All the Ni_2Al_3 coated samples where polished prior to exposure. The main part of the surface was covered by a smooth surface as can be seen in Figure 30. The grain size of the Ni_2Al_3 coating varies over the surface. In some regions the grains are up to 20 μ m while other regions has a grain size of about 5 μ m (as shown in Figure 30).



Figure 30: SEM BSE image of a polished Ni₂Al₃ sample prior to exposure.

In some regions of each sample there were unpolished sections of the surface, see Figure 31. All these regions where shallow and the non-polished pits did not penetrate through the Ni_2Al_3 coating on any position on the samples exposed with or without KCl.

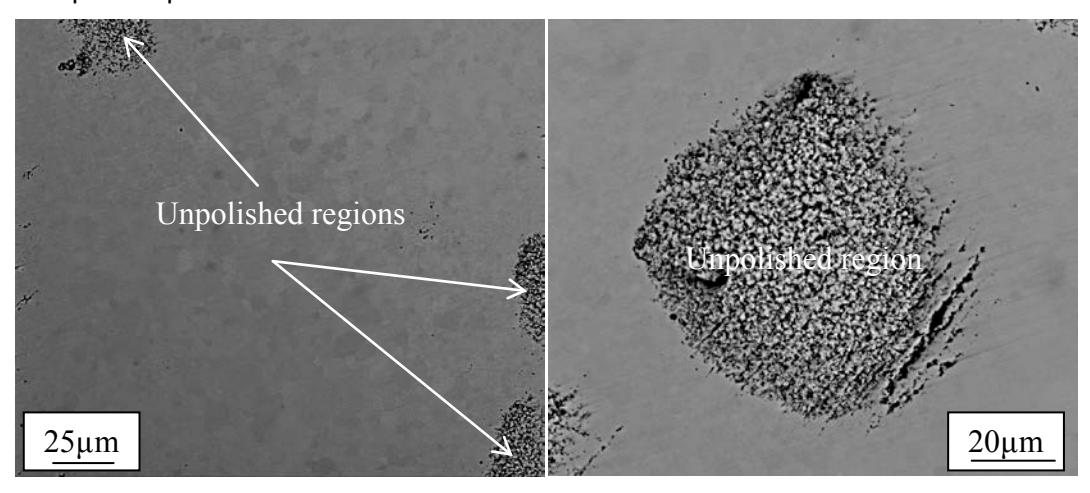


Figure 31 SEM BSE image of a polished Ni_2Al_3 sample prior to exposure showing some unpolished regions.

In the absence of KCl the Ni_2Al_3 coated samples shows a very small mass gain, see Figure 18. XRD showed the presence of the Ni_2Al_3 phase, however the phase of the very thin oxide scale was difficult to identify. After one hour of exposure the sample surface was covered with very thin smooth oxide scale, see Figure 32. As the sample is covered with a very thin oxide scale the surface morphology appearances very similar to the unexposed sample both on the polished and un-polished regions in the SEM image.

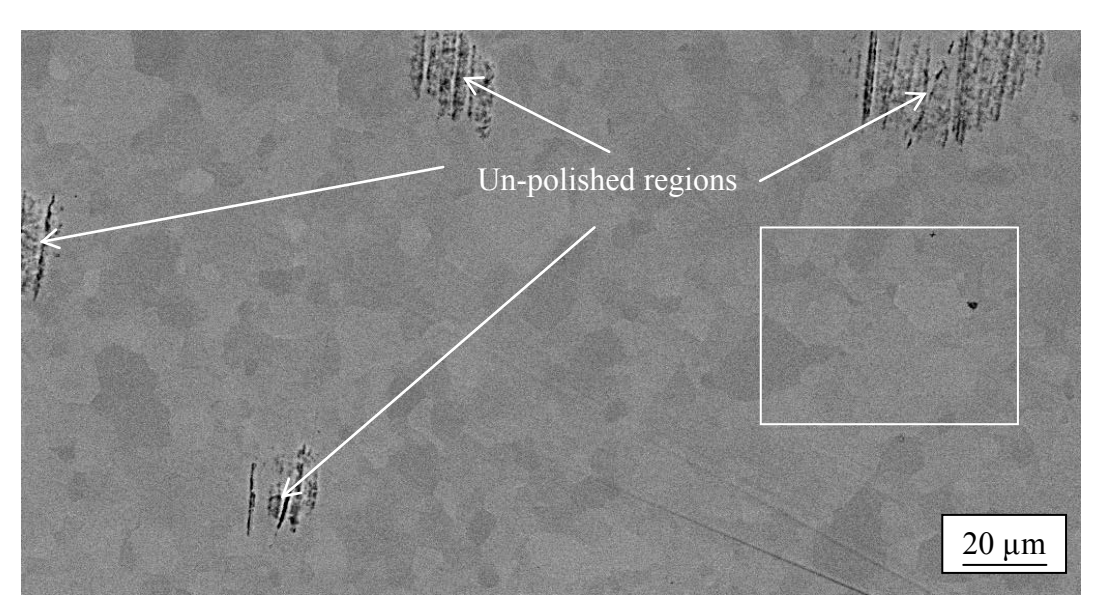


Figure 32: SEM BSE image of Ni_2Al_3 sample exposed at 600 °C for 1h. The marked region corresponds to Figure 33.

The high magnification SE image (Figure 33) shows the thin scale and especially the underlying Ni_2Al_3 grain structure due to channelling of the electrons.

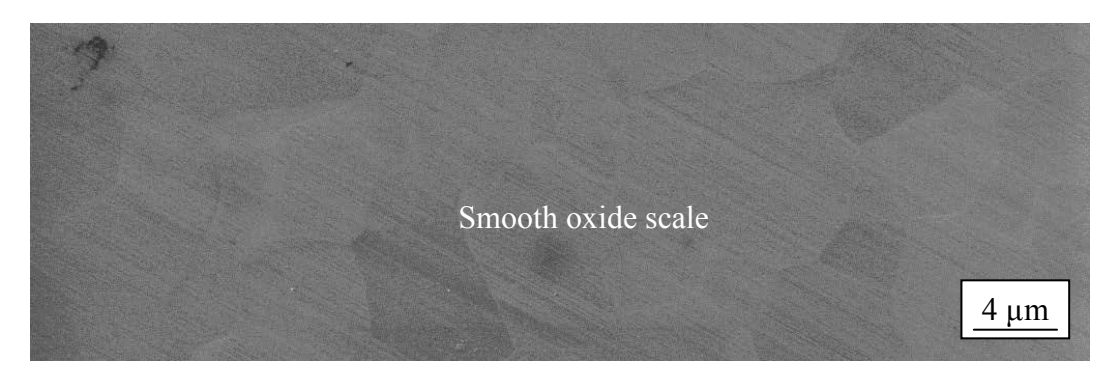


Figure 33: SEM SE image of Ni_2Al_3 sample exposed at 600 °C for 1h.

After 24 hours exposure the oxide scale is still thin and transparent for the electron beam in the SEM, see Figure 34. However, the polished parts of the surface appear to have a more undulating surface morphology. This makes the grain structure of the Ni_2Al_3 coating more apparent. There is a very small difference in contrast between grains in the BSE image indicating a very small difference in oxide scale thickness on different grains.

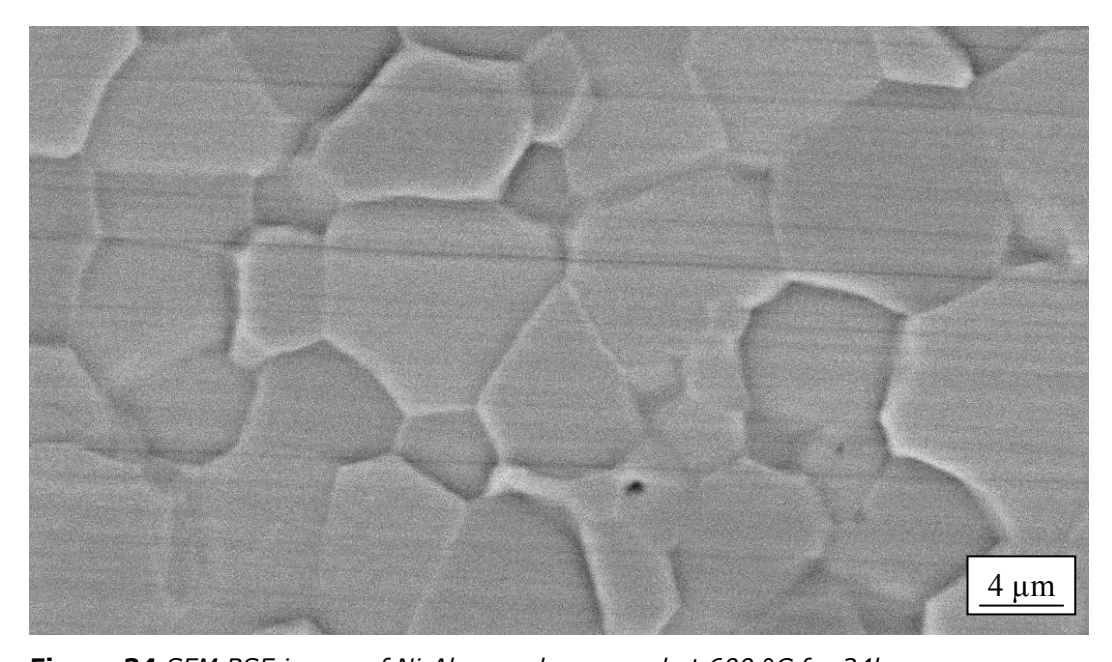


Figure 34 SEM BSE image of Ni_2Al_3 sample exposed at 600 °C for 24h.

The sample exposed for 168 hours have an even more undulating surface morphology than the 24 hours sample, see Figure 35. The Ni_2Al_3 grains are undulating while the grey scale in the BSE image again is similar indicating a similar thickness of the oxide scale on different grains.

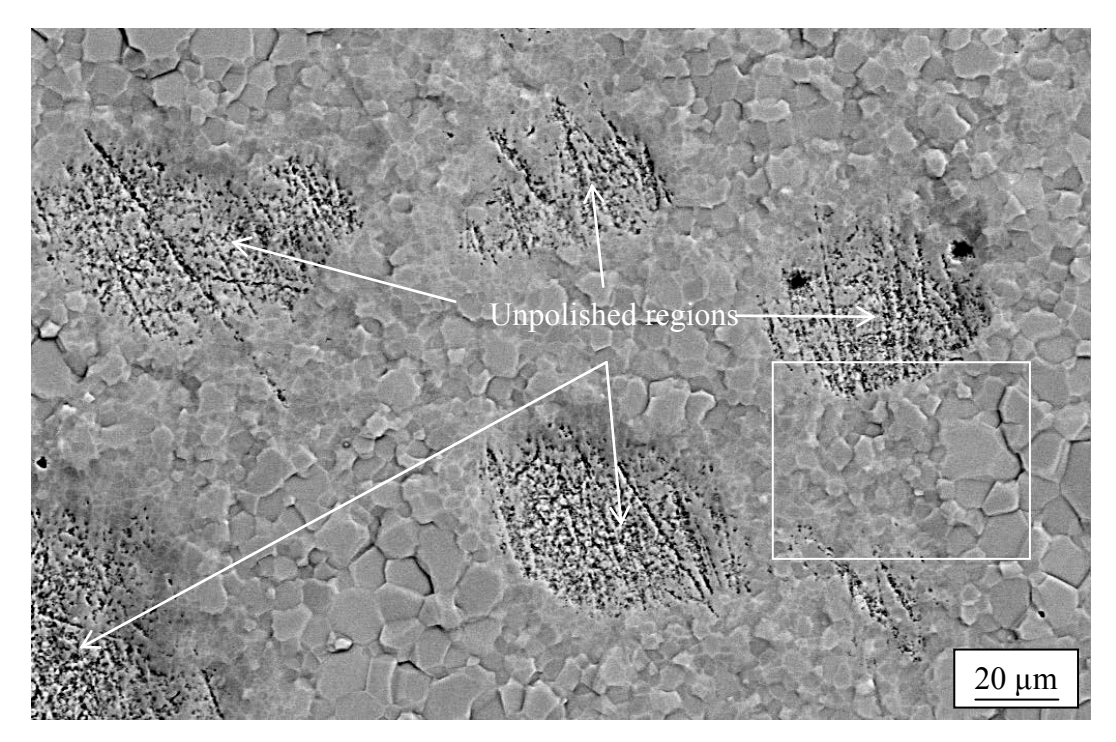


Figure 35: SEM BSE image of Ni_2AI_3 sample exposed at 600 °C for 168h. The marked region corresponds to Figure 36.

Figure 36 shows the former polished region and an un-polished region in higher magnification. The undulating surface of the polished region is apparent and there are no indications of a thicker oxide scale on the unpolished region.

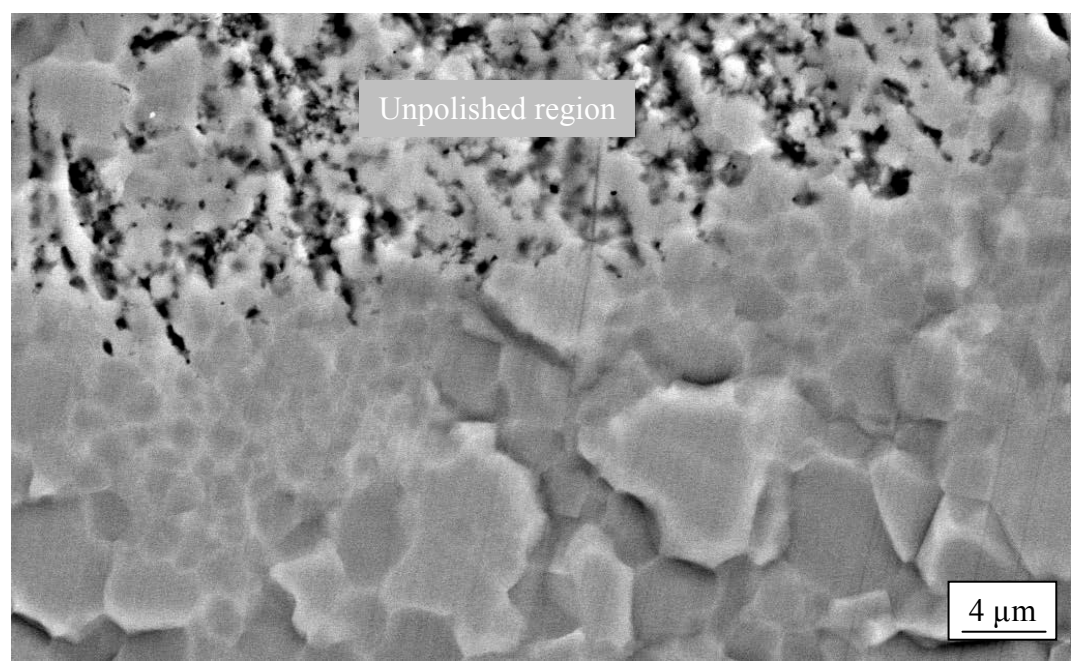


Figure 36: SEM BSE image of Ni_2Al_3 sample exposed at 600 °C for 168h.

In the presence of KCl the Ni_2Al_3 coated sample shows a mass loss, see Figure 18. The mass loss corresponds to the evaporation of KCl. XRD again shows the presence of the Ni_2Al_3 but the phase of the very thin oxide scale was not identifiable. KCl was detected on the sample exposed for one hour. However, in contrast to the exposures of Nickel, oxidation with KCl(s) gives rise to a morphology very similar to that observed on the samples exposed without KCl. Thus, the low magnification image in Figure 37 shows a thin oxide scale all over the parts of the surface with KCl particles on top of the surface. It may be noted that all KCl particles are located on top of un-polished parts of the surface. This does not influence the oxide morphology of these regions.

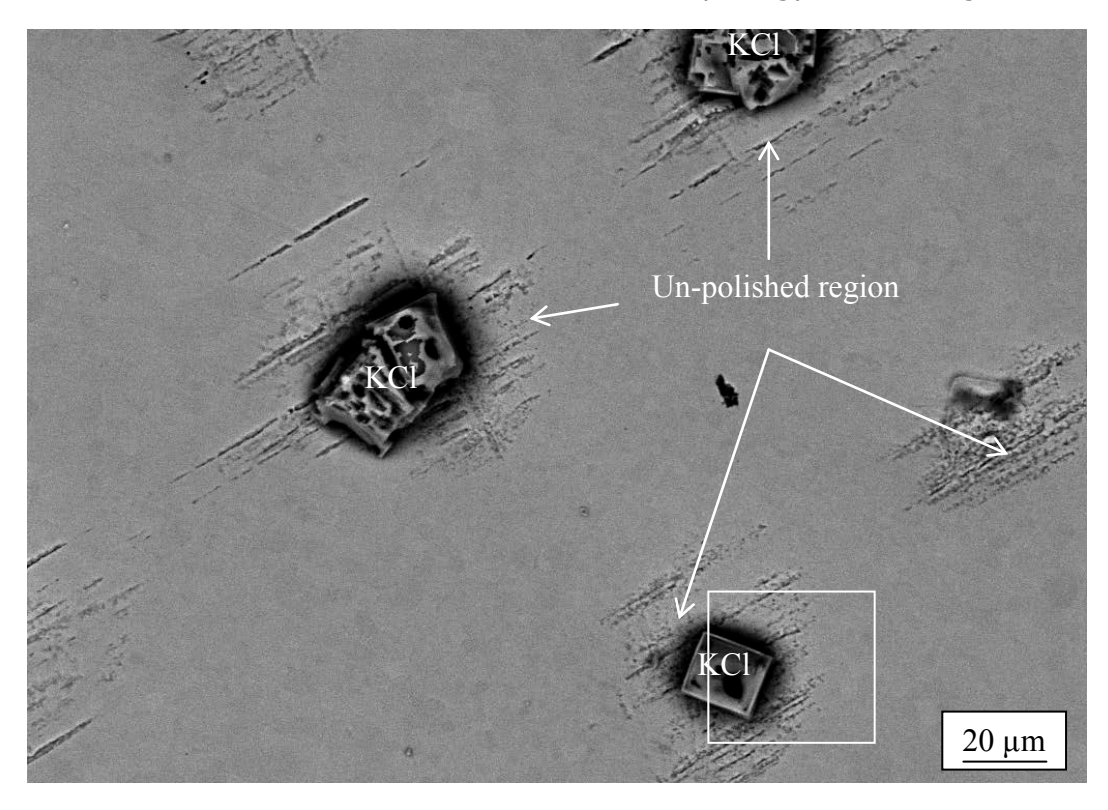


Figure 37 SEM BSE image of Ni_2Al_3 sample exposed with KCl at 600 °C for 1h. The marked region corresponds to Figure 37.

Figure 38 shows an SE image of a KCl particle on top of an un-polished part of the surface. No indications of an oxide rim could be observed in the vicinity of the KCl particle.

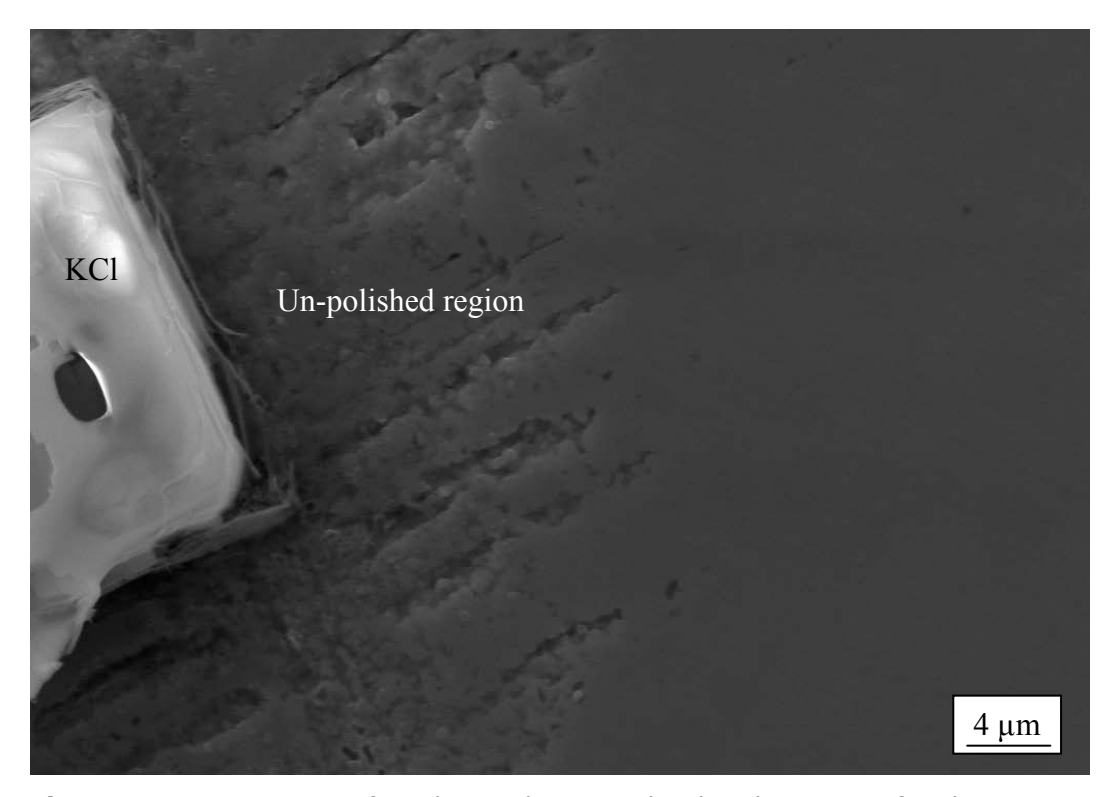


Figure 38 SEM SE image of Ni_2AI_3 sample exposed with KCl at 600 °C for 1h.

After 24 hours exposure most of the KCl has vanished due to evaporation leaving some particles, see Figure 39. No indication of spallation was observed.

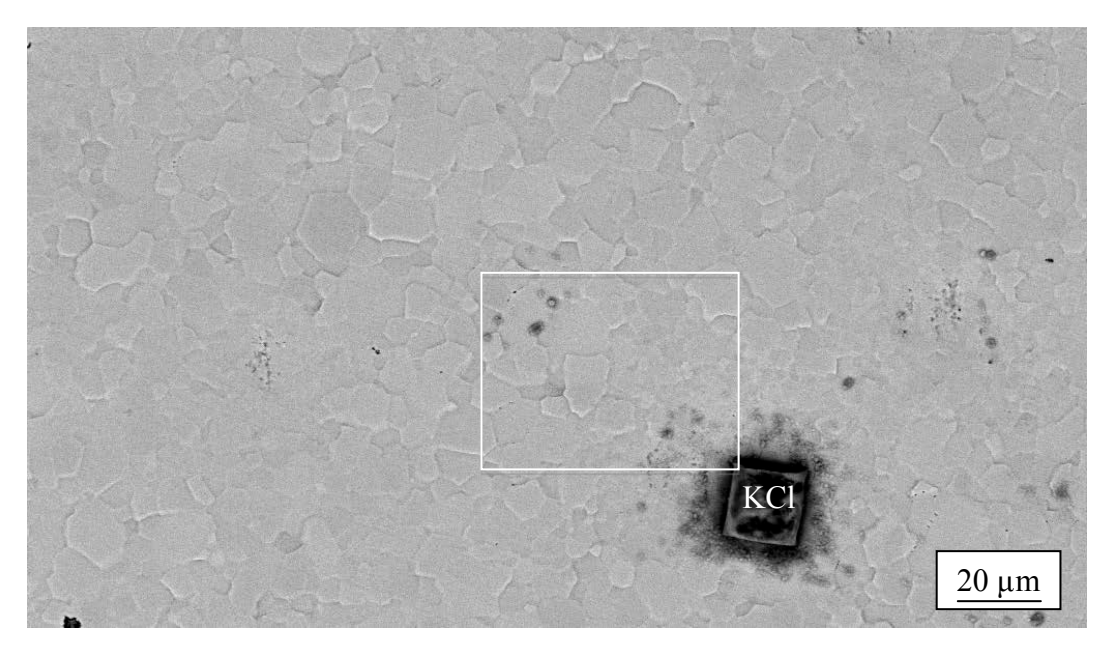


Figure 39: SEM BSE image of Ni_2Al_3 sample exposed with KCl at 600 °C for 24h. The marked region corresponds to Figure 40.

A high magnification SE image of the marked region in Figure 39 shows the vicinity of a remaining KCl particle, see Figure 40. Small KCl particles could be observed but no indications of an oxide rim could be observed. The oxide scale is still thin and transparent for the electron beam in the SEM. However, the polished parts of the surface appear to have a more undulating surface morphology as was observed on the samples exposed for 24 hours without KCl. This makes the grain size of the Ni_2Al_3 coating more apparent.

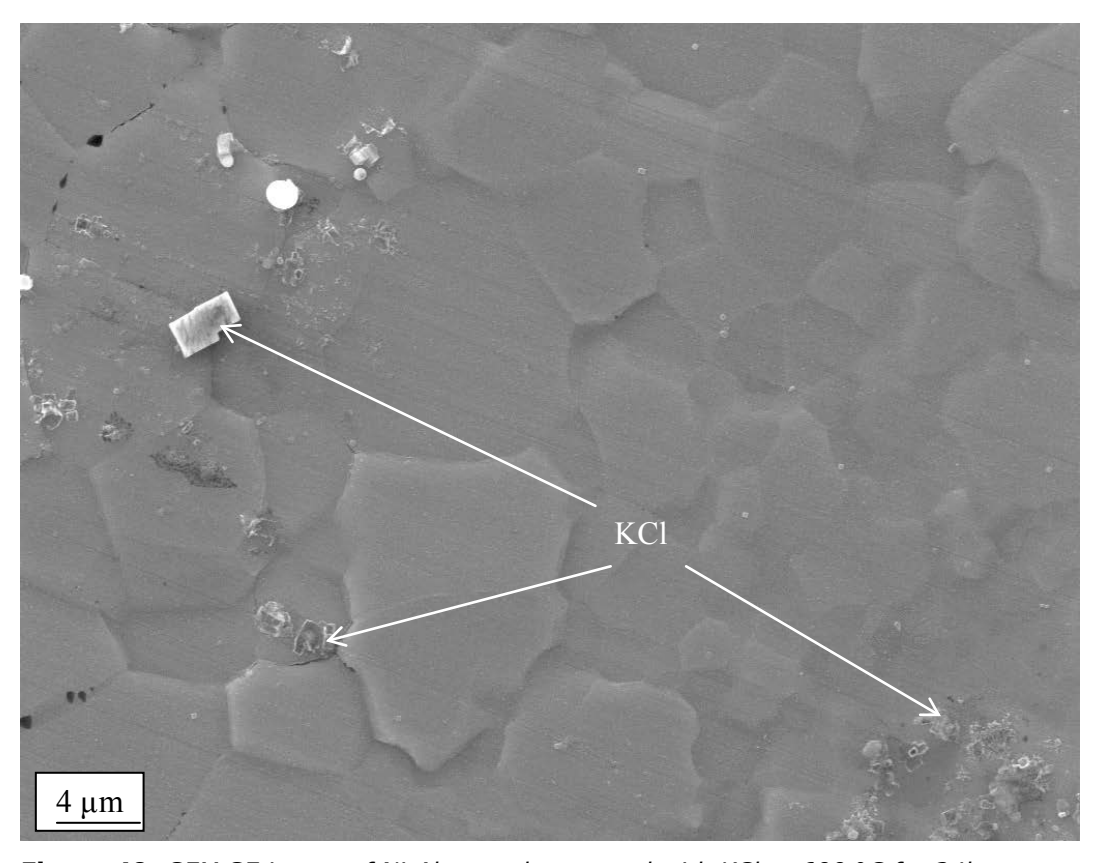


Figure 40: SEM SE image of Ni₂Al₃ sample exposed with KCl at 600 °C for 24h.

The sample exposed for 168 hours still have very few KCl particles present, see Figure 41. However most parts of the surface look very similar to the sample surface of the samples exposed without KCl after 168 hours. The $\rm Ni_2Al_3$ grains have an undulating surface morphology while the grey scale in the BSE image is similar indicating a similar thickness of the oxide scale on different grains.

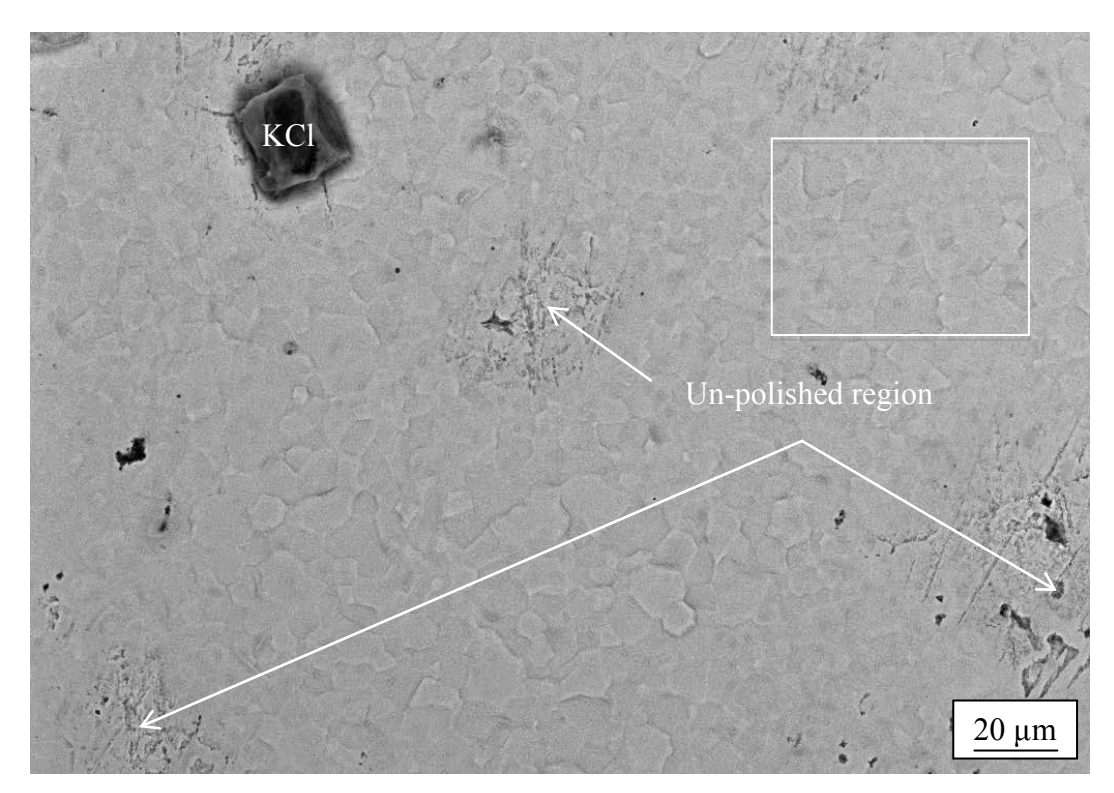


Figure 41: SEM BSE image of Ni_2Al_3 coated sample exposed with KCl at 600 °C for 168h. The marked region corresponds to Figure 42.

Figure 42 shows the former polished region in higher magnification. The undulating surface of the polished region is apparent and there are no indications of a thicker oxide scale on the un-polished region. However small variations in thickness seen as small-elongated nodules a few hundred nm in length could be observed. This was not the case of the samples exposed without KCI.

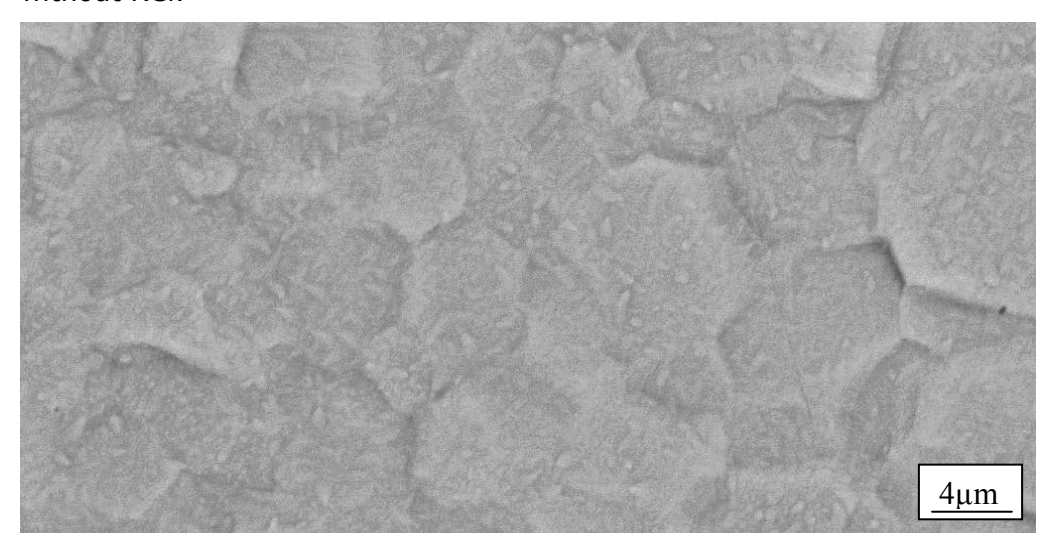


Figure 42: SEM BSE image of Ni_2Al_3 coated sample exposed with KCl at 600 °C for 168h.

A BIB cross-section was ion milled through the oxide scale and into the coating on a Ni_2Al_3 coated sample exposed for 168h in the presence of KCl. In Figure 43 a SEM BSE images depictures the cross-section. The oxide scale is too thin to be observed in the cross-section while the different Ni-Al layers could be observed. The Ni_2Al_3 layer is about 30 μm thick and has a grain size of about 15 μm . Beneath the Ni_2Al_3 layer a 5 μm thick middle layer with composition corresponding to β -NiAl could be identified. The grain size of this layer is about 10 μm . The 10 μm thick bottom layer consist of 70 at.% Ni and 30 at.% Al and has a grain size of about 3 μm . There may be more layers present in-between the observed layers but they are in that case thin and difficult to resolve with the SEM/EDX. According to the Ni-Al phase diagram, both Ni_5Al_3 and Ni_3Al can be expected to form. None of the layers contains any voids in the ion-milled cross-section.

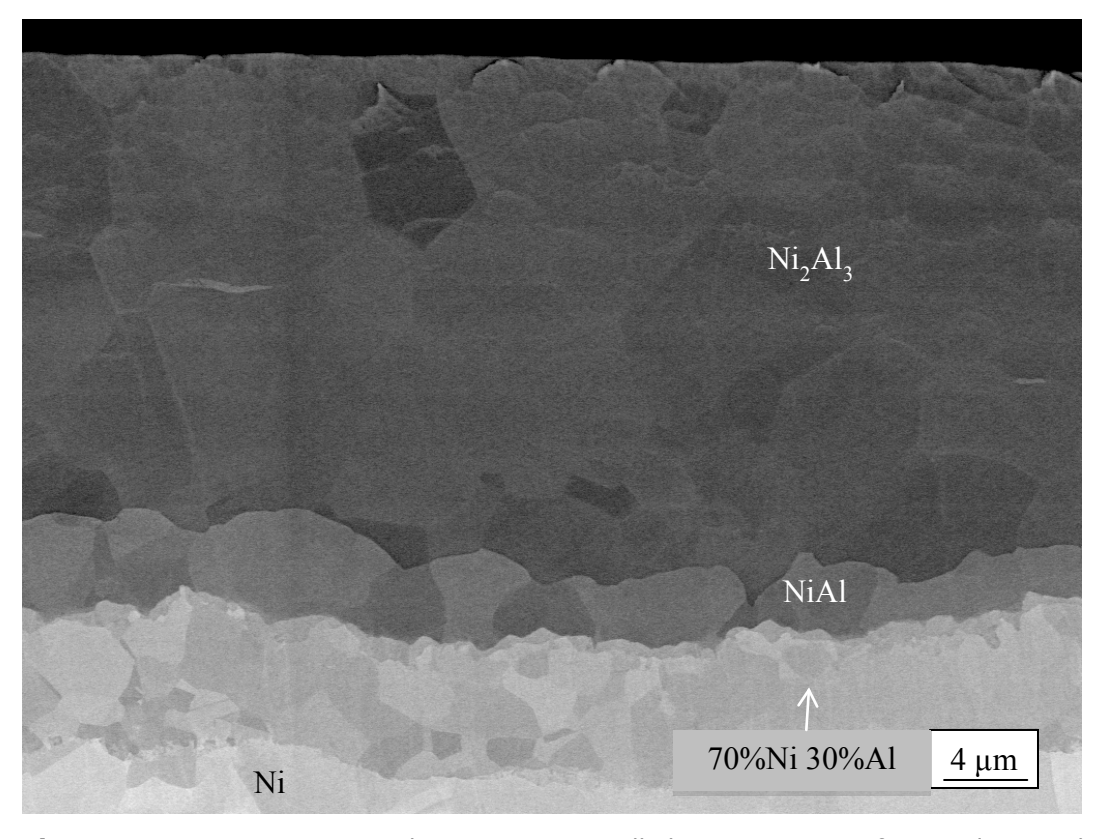


Figure 43: SEM BSE image showing an ion milled cross-section of a Ni_2Al_3 coated sample exposed with KCl at 600 °C for 168h.

In order to investigate the thin protective scale after 168 hours in the presence of KCl a TEM sample was prepared with FIB/SEM. Figure 44 shows a TEM BF image of the oxide scale and subjacent Ni_2Al_3 coating. The oxide scale is 50nm-250nm in the cross-section, which is in the line with the calculated thickness of the oxide scale (190nm on the sample exposed without KCl). The grain size of the Ni_2Al_3 coating is a few μm in this section and the undulating surface indicated in the top view images after 168 hours exposure could be confirmed. The nodules seen on the surface likely correspond to the small-elongated nodules seen in the SEM, cf. Figure 42.

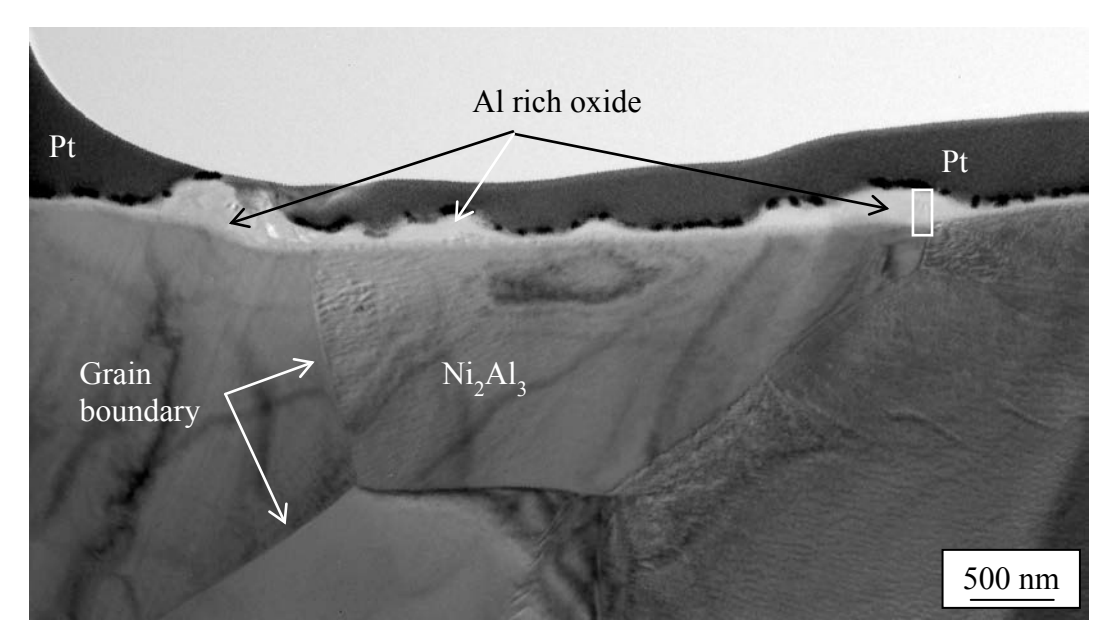


Figure 44: TEM BF image showing the thin oxide scale in cross-section of a Ni_2Al_3 coated sample exposed with KCl at 600 °C for 168h. The EDX profile shown in Figure 45 was measured in the marked region.

The electron transparent oxide scale was difficult to analyse by TEM/EDX and diffraction due to the interaction between electron beam and oxide. The EDX spot measurements resulted in burn-through of the thin oxide, but still reveal that the oxide scale contains O, Al, K and a small amount of Ni, see the results of EDX measurements in Figure 45. Only cations content is plotted in the EDX profiles since oxygen is difficult to quantify. The oxygen content was measured to about 50 at.% in the oxide scale. The outermost part of the nodule is enriched in Ni, followed by a section enriched in K, near the interface to the $\mathrm{Ni_2Al_3}$, the K content drops. The morphology of this zone is also slightly different from the bulk nodule. No measurable Al depletion in the bulk could be found.

Diffraction carried out in the middle section of a nodule was consistent with the presence of a $K_xAl_yO_z$ phase. The fall in K towards the interface to the bulk alloy, could indicate the formation of a more Al-rich oxide at the interface. This could be Al_2O_3 but it was not confirmed.

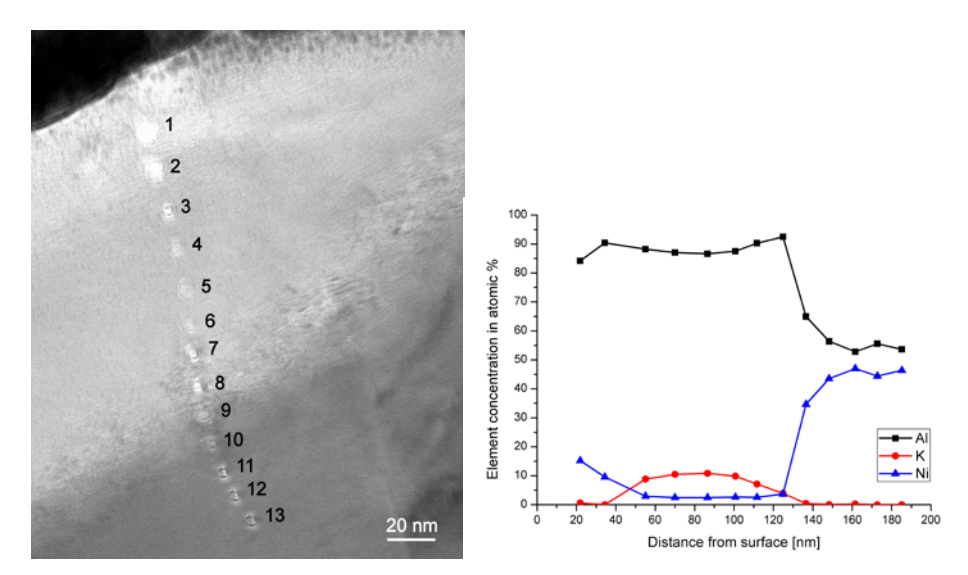


Figure 45: TEM BF image showing EDX measurement points in the thin oxide scale in cross-section of a Ni_2Al_3 coated sample exposed with KCl at 600 °C for 168h. EDX results are shown in at% in the line profile, oxygen signal and signal from deposited gold and copper grid was removed in the quantification.

On one of the Ni_2Al_3 coated samples exposed for 168 hours with KCl cracks was observed close to the edge of the sample, see Figure 46. The cracks were up to 10 μ m wide and on some positions Si rich oxide could be found in and in the vicinity of the crack. This indicates that the cracks had been present prior to exposure and that silicon carbide was pushed into the crack during polishing of the sample prior to the exposure. The crack formation could indicate some brittleness of the intermetallic Ni_2Al_3 phase. Despite the crack no fast corrosion occurred and there was no large difference in mass gain compared to the other samples.

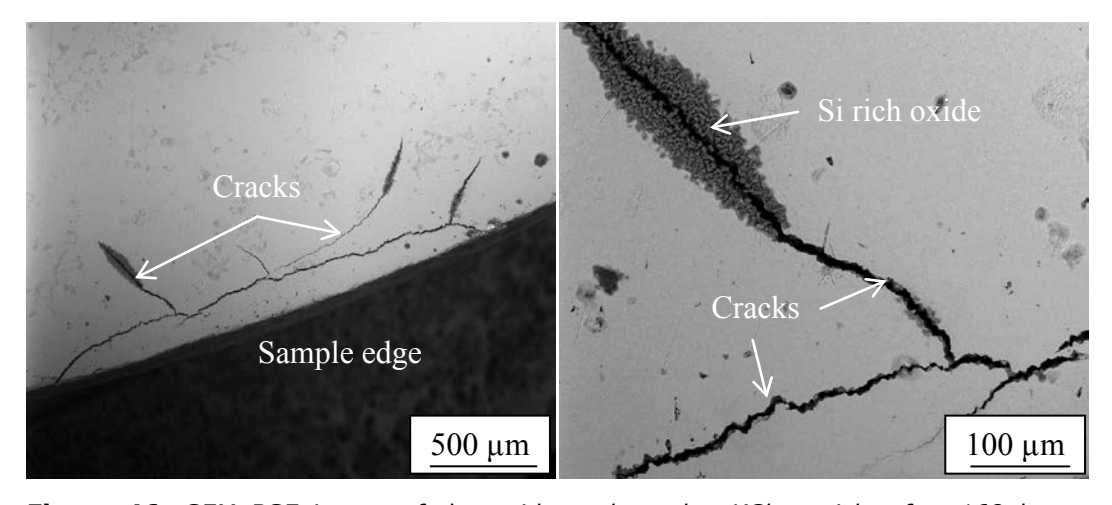


Figure 46: SEM BSE image of the oxide scale and a KCl particle after 168 hours exposure. The main part of the sample is covered with at smooth oxide scale but a large crack was observed close to one edge.

5.4 Summary

The detailed investigation of the oxidation of the stainless steel samples and the microstructure before and after breakdown gives important information about the influence of KCl on chromia. The stainless steel forms a protective scale to start with. The scale is rich in chromium and very slow growing even though KCl reacts with the oxide scale forming $K_2 CrO_4$ already after a very short time, thus depleting the scale in chromium. As the level of chromium falls below a critical concentration breakaway oxidation occurs. This happened within 1h at 600°C. After breakaway oxidation the microstructural investigation reveals an outward growing iron oxide as well as an inward growing Fe,Cr,Ni spinel oxide. Thus, small amounts of alkali may transform a protective oxide scale to a non-protective scale in a very short time span at 600 °C.

Oxidation of pure Nickel gives a similar mass gain rate as the stainless steel after breakdown of the protective chromium rich oxide, see Figure 18. The results indicate that addition of small amounts of KCl does not increase the growth rate on pure Nickel at 600 °C. However, the surface morphology changes around the KCl particles. No indication of other phases was detected with XRD or SEM/EDX. Neither was any potassium or chloride detected in the oxide scale even though the scale was very porous after 168 hours exposure in the presence of KCl, see Figure 29.

Both the mass gain and the microstructural investigation of the Ni₂Al₃ coated samples confirm that the Ni₂Al₃ coating forms a protective aluminium rich oxide scale in all environments and after all exposure times. There are no indications of crust formation around the KCl particles when deposited on the Ni₂Al₃ coated samples. The results in addition indicate that the KCl evaporates somewhat slower than on the Nickel and stainless steel samples. The microstructure investigation indicates the formation of $K_xAl_yO_z$ phase growing in nodules on the surface, the K content falls towards the interface to the bulk alloy, indicating the formation of a more Al-rich oxide at the interface. This could be Al₂O₃ but it was not confirmed. The morphology of the polished surface becomes undulating with longer exposure times (compare e.g. Figure 32 and Figure 35). With longer exposure times the NiAl layer beneath the Ni₂Al₃ coating also grows as well as a more Ni rich layer forms (likely Ni₂Al₅ or Ni₃Al). A crack was observed on one of the Ni₂Al₃ coated sample close to the edge of the sample see Figure 46. The results indicate that the cracks had been present prior to the exposure. It could indicate some brittleness of the Ni₂Al₃ phase. Despite the crack no fast corrosion occurred and there were no large difference in mass gain compared to the other samples.

6 Analysis of the results

One way to reduce CO_2 emissions is to convert PF (pulverised fuel) SC (supercritical) boilers from fossil-firing (coal or gas) to biomass-firing, e.g. wood or straw. Biomass is much more corrosive than fossil fuels, and thus the outlet steam temperature of converted units most likely needs to be lowered in order to obtain acceptable corrosion rates. The accelerated corrosion due to the more corrosive fuel has been identified as the major materials challenge in this conversion, severely decreasing the lifetime of e.g. the superheaters in the boiler. Increased knowledge of the alkali chloride induced corrosion as well as identification of coating/materials that can resist the environment is essential for forming a platform for the conversion of boilers as described above.

The present project aims to increase the fundamental knowledge of the general corrosion mechanism as well as identify alternative materials solutions that minimize superheater corrosion in boilers with advanced steam data. The results will contribute to the understanding of how a power plant with advanced steam data can be operated with different types of fuel quality. The obtained knowledge can directly benefit boiler operators by allowing them to make optimum materials choices and thereby increase steam data and/or lifetime of critical components.

The project can be divided into three major parts, namely the detailed investigation of field samples, thermodynamic calculations combined with oxide screening experiments and finally laboratory studies of the most promising materials system. From the detailed investigation of field exposed samples it is clear that an 18-8 type of stainless steel such as the TP347HFG material is not able to form a protective chromia scale under the present superheater service conditions. Extensive attack is found along grain boundaries with both K and Cl present in the boundaries and presumably both being active at the corrosion front. The transmission electron investigations reveal that the formed oxide is inhomogeneous on a nanoscale. The interpretation of the corrosion attack is complex due to the simultaneous presence of several degradation mechanisms. It is clear that also sulphur and not only potassium and chlorine could be found in the complex corrosion products after breakdown of the protective scale. It is however believed that the initial reaction between potassium and chromia oxide to form potassium chromate is the main reason for the TP347HFG steel not being able to form a protective oxide under the service conditions [21-23]. This is supported by the results from the lab study of the stainless steel 304L.

Adding small amounts of KCl ($0.10~\text{mg/cm}^2$) to the surface of steel 304L generates a breakdown of the protective scale in a very short time span (1h) over large parts of the surface. The breakdown mechanism being the formation of $K_2\text{CrO}_4$ depleting the Cr rich oxide in chromium. This results in a chromium poor oxide and breakaway oxidation giving an outward growing iron rich oxide and a inward growing Cr,Fe,Ni oxide. The investigated field

samples have formed a comparable non-protective scale with a similar microstructure also after the long exposure time (5900 hours), compare Figure 1 and Figure 22. The detailed investigation of the lab samples and the microstructure after breakdown may in addition explain the complex microstructure formed after longer exposure times on the field samples. The non-protective fast growing scale may open diffusion paths not only for oxygen but also for e.g. chlorine and sulphur from the deposit resulting in the complex microstructure observed in the detailed investigation of the field samples, see e.g. Figure 6. It may therefore be concluded that the stainless steel does not form a protective scale and that the scales formed are fast growing and penetrable for e.g. chlorine and sulphur from the deposit. This information was taken into account setting up the thermodynamic calculations.

Based on the observations from field tests and the laboratory exposures of 304L the first step in identifying candidate materials solutions was to evaluate the resistance against oxygen, chlorine and potassium. A number of candidate alloying systems were identified based on calculated M-O₂-Cl₂ diagrams and oxide screening experiments testing the interaction of oxides with KCl. It was confirmed that chromia was unsuited as protective oxide, due to the interaction with potassium and formation of K_2CrO_4 . No interaction with Al_2O_3 was observable and therefore the Ni-Al system and specifically the Ni_2Al_3 intermetallic phase was chosen for laboratory testing. Nickel was chosen as matrix material due to the large metal stability area in the calculated $Ni-O_2-Cl_2$ diagrams.

The behaviour of the matrix material Nickel is important to investigate in order to better understand the Ni-Al system and to know the oxidation behaviour if the coating becomes depleted in Al. Oxidation of Nickel gives a similar growth rate as the stainless steel after breakdown of the protective chromium rich oxide scale, see Figure 18. The results indicate the addition of small amounts of KCl do not increase the growth rate. However, the surface morphology changes around the KCl particles. This is very similar to the build up of oxide crust around KCI particles on low-alloyed steels and stainless steels even though it is not as pronounced, see e.g. [21]. The formation of crusts around KCl particles has been explained by the formation of eutectic FeCl₂KCl mixture, which has a eutectic temperature of 355 °C, formation on the surface [34]. Examining the NiCl₂-KCl system shows a similar eutectic but at considerably higher temperature (at 514 °C), see Figure 47. This difference in temperature may explain the much smaller crusts on Nickel compared to the crusts formed on the low alloyed and stainless steels, compare Figure 20 and Figure 25. The results indicate that the formation of the eutectic do not strongly influence the growth rate of Nickel at 600 °C under the present conditions. No indication of other phases was detected with XRD or SEM/EDX. Neither was any potassium or chloride in the oxide scale even though the scale was very porous after 168 hours exposure in the presence of KCI, see Figure 29.

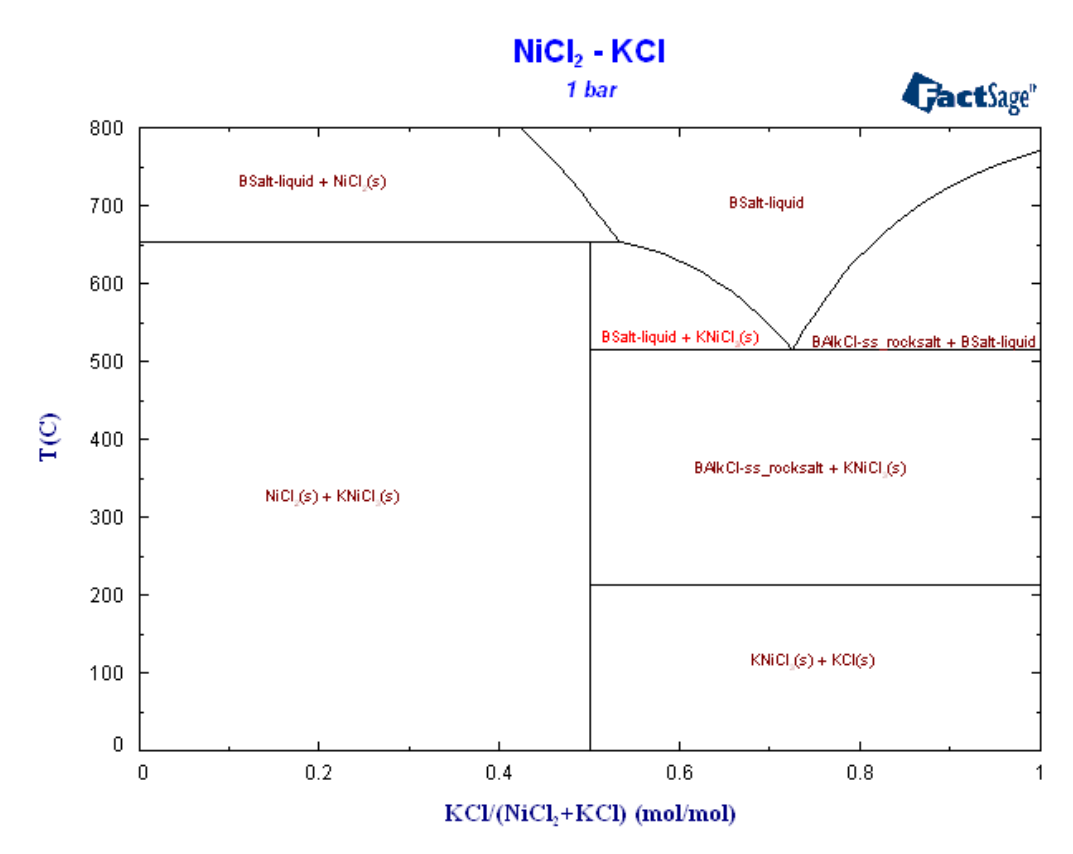


Figure 47: A KCl- NiCl₂ phase diagram calculated with Factsage.

Both the mass gain and the microstructure investigation confirm that the Ni₂Al₃ coating forms a protective aluminium rich oxide scale in all environments and after all exposure times. The growth rate is in addition similar to that of protective chromium rich oxide scale formed on stainless steels even though an alpha Al₂O₃ not forms at 600°C. There are no indications of crust formation around the KCl particles. The results in addition indicate that the KCI evaporates somewhat slower than on the Nickel and stainless steels. This may be explained by a more passive surface beneath and around the particles. Neither is a KCI-AlCl₃ eutectic expected to form and thereby transporting the KCl over the surface, which may slow down the evaporation. This since the amount of AlCl₃ is expected to be low on the surface because the vapour pressure of AlCl₃ is very high (PAlCl₃=0.667 atm at 600 °C) compared to the vapour pressure of FeCl₂ (PFeCl₂=1.00E-03 atm at 600 °C). The microstructure investigation shows the formation of an aluminium rich oxide phase also in the presence of KCl. The phase has not been possible to identify but it is slow growing and only small amounts of potassium could be found in the scale. The results indicate that the potassium do not influence the diffusion through the scale. The morphology of the polished surface becomes undulating with longer exposure times (compare e.g. Figure 32 and Figure 35). There are no indications that this influences the oxide scale on top the Ni₂Al₃ grains or in at the grain boundaries. With longer exposure times the β-NiAl layer beneath the Ni₂Al₃ coating grows and a more Ni rich layer forms. This information may be used to extrapolate the depletion

of Al from the $\mathrm{Ni_2Al_3}$ coating. A crack was observed on one of the $\mathrm{Ni_2Al_3}$ coated sample close to the edge of the sample see Figure 46. The results indicate that the cracks had been present prior to the exposure. Despite the crack no fast corrosion occurred and there were no large difference in mass gain compared to the other samples. Thus, the Ni-Al system shows a large potential for formation of a protective aluminium scale in the alkali chloride-containing environment used in the lab.

7 Conclusions

- Characterization of TP347HFG superheater samples revealed that the steel was not able to form a protective chromia scale under the superheater service conditions and long exposure times.
- It was concluded that the major breakdown mechanism was the reaction between K and Cr-rich oxide to form K₂CrO₄. This was based on both the detailed laboratory investigation of stainless steel and the detailed investigation of field stainless steel samples.
- Thermodynamic evaluations using Thermo-Calc combined with oxide screening experiments identified the Ni-Al system to have large potential in an alkali chloride rich environment.
- The Ni_2AI_3 intermetallic phase has been produced on pure Ni at DTU using pack cementation. The aluminising led to formation of a $\sim 30~\mu m$ thick layer of Ni_2AI_3 .
- The Ni-Al system shows a large potential for formation of a protective aluminium scale in the alkali chloride-containing environment used in the lab. In the lab environment containing small amounts of KCl the 304L stainless steel goes into breakaway corrosion while the Ni₂Al₃ coating forms a thin aluminium rich protective oxide scale.

8 Goal fulfilment

The overall goal of the present project is to identify a possible material for superheater tubes, which allows an outlet steam temperature of at least 580°C on biomass converted fossil-fired units. The corrosive properties of biomass fuels such as wood and straw have mainly been attributed to the high alkali chlorine content. By studying field exposed samples and performing thermodynamic calculations the Ni-Al material system was identified as a possible alkali chloride resistant coating material. The results from the laboratory exposures show that the Ni₂Al₃ coating resisted the initial attack of KCl. The Ni-Al system has thereby been shown to be a potential coating system in alkali chloride rich environments. The results have in addition generated an interest among boiler owners and there are expectations to further test the Ni-Al system. The goal of the project has thereby been fulfilled.

9 Suggestions for future research work

This project was a first step in investigating possible coatings/materials in alkali chloride rich environments combining field test, thermodynamic evaluations and laboratory studies. The results have enlightened various aspects and possibilities and identified both a potential material system as well as a work procedure to achieve this. The results obtained within the project have also raised many suggestions for further studies. More work is needed to further study the Ni-Al system: Longer exposure times, thermal cycling, larger amounts of applied KCl, effect of sulphur and loss of aluminium through interdiffusion as well as mechanical properties of the coatings need to be tested. The effect of the Al to Ni ratio in the coating could also be evaluated in order to investigate whether $\mathrm{Ni_2Al_3}$ or $\beta\text{-NiAl}$ coatings are the most promising. In order to implement the coatings in a real boiler additional work is also needed, including in-plant testing as well as identifying the most suitable method for application of such coatings.

10 Literature references

- 1. Larsen, O.H. and M. Montgomery, *Materials Problems and Solutions in Biomass Fired Plant*. Materials Science and Engineering for Energy Systems, 2006. **1**(4): p. 227-237.
- 2. Montgomery, M., et al., Experiences with high temperature corrosion at straw-firing power plants in Denmark. Materials and Corrosion-Werkstoffe Und Korrosion, 2011. **62**(7): p. 593-605.
- 3. Lee, S.Y. and M.J. McNallan, *Inhibition of Oxidation of Iron in Environments Containing Chlorine at 1100-K and 1200-K.* Journal of the Electrochemical Society, 1990. **137**(2): p. 472-479.
- 4. Lee, S.Y. and M.J. McNallan, Formation of Condensed Chlorides During Mixed Oxidation Chlorination of Iron at 1000-K. Corrosion, 1991. **47**(11): p. 868-874.
- 5. Lee, Y.Y. and M.J. McNallan, *Ignition of Nickel in Environments Containing Oxygen and Chlorine*. Metallurgical Transactions a-Physical Metallurgy and Materials Science, 1987. **18**(6): p. 1099-1107.
- 6. McNallan, M.J., et al., *Accelleration of the High Temperature Oxidation of Metals by Chlorine.* High Temperature Corrosion, NACE, 1983: p. 316-321.
- 7. Stott, F.H. and C.Y. Shih, *The influence of HCl on the oxidation of iron at elevated temperatures.* Materials and Corrosion, 2000. **51**(5): p. 277-286.
- 8. Abels, J.-M. and H.-H. Strehblow, A Surface Analytical Approach to the High Temperature Chlorination Behaviour of Inconel 600 at 700°C. Corrosion Science, 1997. **39**(1): p. 115 132.
- 9. Bender, R. and M. Schutze, *The role of alloying elements in commercial alloys for corrosion resistance in oxidizing-chloridizing atmospheres Part II: Experimental investigations.* Materials and Corrosion, 2003. **54**(9): p. 652-686.
- 10. Grabke, H.J., E. Reese, and M. Spiegel, *The Effects of Chlorides, Hydrogen-Chloride, and Sulfur-Dioxide in the Oxidation of Steels Below Deposits.* Corrosion Science, 1995. **37**(7): p. 1023-1043.
- 11. Haanappel, V.A.C., et al., *Corrosion Kinetics of Low-Alloy and High-Alloy Steels in Chlorine-Containing Gas Atmospheres.* Corrosion, 1992. **48**(10): p. 812-821.
- 12. Kim, A.S. and M.J. McNallan, *Mixed Oxidation of Iron Chromium-Alloys in Gases Containing Oxygen and Chlorine at 900 to 1200-Degrees-K.* Corrosion, 1990. **46**(9): p. 746-755.
- 13. Liu, J.C. and M.J. McNallan, *Effects of temperature variations on oxidation of iron-20% chromium alloys at 1200 K in Ar-20% O-2-Cl-2 gas mixtures.* Materials and Corrosion, 1999. **50**(5): p. 253-260.
- 14. Sroda, S., et al., *High temperature oxidation behaviour of boiler steels under simulated combustion gases.* Materials Science Forum, 2004. **461-464**: p. 981-988.
- 15. Stott, F.H. and C.Y. Shih, *High-temperature corrosion of iron-chromium alloys in oxidizing-chloridizing conditions.* Oxidation of Metals, 2000. **54**(5-6): p. 425-443.

- 16. Sämann, N., M. Spiegel, and H.J. Grabke, *Influence of surface preparation on the corrosion of steels in simulated waste incineration environments.* Materials Science Forum, 2001. **369-3**: p. 963-970.
- 17. Zahs, A., M. Spiegel, and H.J. Grabke, *The influence of alloying elements on the chlorine-induced high temperature corrosion of Fe-Cr alloys in oxidizing atmospheres.* Materials and Corrosion, 1999. **50**(10): p. 561-578.
- 18. Zahs, A., M. Spiegel, and H.J. Grabke, *Chloridation and oxidation of iron, chromium, nickel and their alloys in chloridizing and oxidizing atmospheres at 400-700 degrees C.* Corrosion Science, 2000. **42**(6): p. 1093-1122.
- 19. Zheng, X.J. and R.A. Rapp, *Chloridation-oxidation of nine commercial high-temperature alloys at 800 degrees C.* Oxidation of Metals, 1997. **48**(5-6): p. 553-596.
- 20. Folkeson, N., Johansson, L. G. and Svensson, J. E., *Initial stages of the HCl-induced high-temperature corrosion of alloy 310.* Journal of the Electrochemical Society, 2007. **154**(9): p. C515-C521.
- 21. Jonsson, T., et al., The influence of KCl on the corrosion of an austenitic stainless steel (304L) in oxidizing humid conditions at 600 °C: A microstructural study. Oxidation of Metals, 2009. **72**(3): p. 213-239.
- 22. Karlsson, S., et al., Alkali Induced High Temperature Corrosion of Stainless Steel: The Influence of NaCl, KCl and CaCl2. Oxidation of Metals, 2012. **78**(1-2): p. 83-102.
- 23. Pettersson, C., J. Pettersson, H. Asteman, J.-E. Svensson and L.-G. Johansson *KCl-induced high temperature corrosion of the austenitic Fe-Cr-Ni alloys 304L and Sanicro 28 at 600°C.* Corrosion Science, 2005. **48**(6): p. 1368-1378.
- 24. Pettersson, J., et al., *The influence of sulphur additions on the corrosive environment in a waste-fired CFB boiler.* High-Temperature Oxidation and Corrosion 2005, 2005. **522-523**: p. 563-570.
- 25. Pettersson, J., et al., *The Influence if Sulphur Additions on the Corrosive Environment in a Waste-Fired CFB Boiler.* Materials Science Forum, 2006. **522-523**: p. 563-570.
- 26. Jonsson, T., et al. Sewage sludge as additive to reduce the initial fireside corrosion caused by combustion of shredder residues in a waste-fired BFB boiler. in 9th Liège Conference on Materials for Advanced Power Engineering. 2010. Liege.
- 27. Andersson, J.O., et al., *Thermo-Calc and DICTRA, Computational tools for materials science.* Calphad, 2002. **26**: p. 273-312.
- 28. Israelsson, N., et al., *KCI-induced corrosion of an FeCrAI alloy at 600* °C in O2 + H2O environment: The effect of pre-oxidation. Submitted to Oxidation of Metals, 2013.
- 29. Israelsson, N., et al., *KCI-induced corrosion of the FeCrAI alloy Kanthal*® *AF at 600 °C and the effect of H2O.* Submitted to Oxidation of Metals, 2013.
- 30. Reed, R.C., *The Superalloys Fundamentals and Applications.* Cambridge University Press, 2006.
- 31. Li, Y.S., M. Spiegel, and S. Shimada, *Corrosion behaviour of various model alloys with NaCl-KCl coating.* Materials Chemistry and Physics, 2005. **93**(1): p. 217-223.

- 32. Wang, J., et al., Low temperature pack aluminizing kinetics of nickel electroplated on creep resistant ferritic steel. Surface & Coatings Technology 2013. **236**: p. 135-141.
- 33. Asteman, H., Svensson, J. E., Norell, M., Johansson, L. G., *Influence of water vapor and flow rate on the high-temperature oxidation of 304L; Effect of chromium oxide hydroxide evaporation.* Oxidation of Metals, 2000. **54**(1-2): p. 11-26.
- 34. Jonsson, T., et al., An ESEM in situ investigation of initial stages of the KCl induced high temperature corrosion of a Fe-2.25Cr-1Mo steel at 400 °C. Corrosion Science, 2011. **53**(6): p. 2233-2246.

11 Publications

The results from the laboratory part have been accepted for oral presentation at the international conference Microscopy of Oxidation 9. A paper will in addition be submitted to Materials at High temperature.

ELFORSK

SVENSKA ELFÖRETAGENS FORSKNINGS- OCH UTVECKLINGS - ELFORSK - AB

Elforsk AB, 101 53 Stockholm. Besöksadress: Olof Palmes Gata 31 Telefon: 08-677 25 30, Telefax: 08-677 25 35 www.elforsk.se